MOLECULAR DYNAMICS SIMULATION OF HYDROGEN ISOTOPES TRAPPING ON TUNGSTEN: THE EFFECT OF PRE-IRRADIATION

by

Enes Ercikan

A Thesis

Submitted to the Faculty of Purdue University

In Partial Fulfillment of the Requirements for the degree of

Master of Science in Nuclear Engineering

School of Nuclear Engineering

West Lafayette, Indiana

December 2019

THE PURDUE UNIVERSITY GRADUATE SCHOOL
STATEMENT OF COMMITTEE APPROVAL

Dr. Tatyana S. Sizyuk, Chair
School of Nuclear Engineering
Dr. Ahmed Hassanein
School of Nuclear Engineering
Dr. Maria A. Okuniewski
School of Materials Engineering

Approved by:

Dr. Seungjin Kim
Head of the Graduate Program

ACKNOWLEDGEMENTS

First and foremost, I would like to thank Dr. Tatyana S. Sizyuk for being my adviser during my study and research. Without her support and guidance, this study would have been more challenging, stressful and time consuming.

Additionally, I would also like to thank all group members of Center for Materials Under eXtreme Environment (CMUXE), both faculties and students, for their valuable suggestions and supports.

Last but not least, my gratitude is extended to my committee members: Dr. Ahmet Hassanein and Dr. Maria A. Okuniewski for their constructive advice.

TABLE OF CONTENTS

LIST OF TABLES

LIST OF FIGURES

ABSTRACT

Author: Ercikan, Enes. MSNE
Institution: Purdue University
Degree Received: December 2019
Title: Molecular Dynamics Simulation of Hydrogen Isotopes: The Effect of Pre-Irradiation.
Committee Chair: Tatyana S. Sizyuk

To achieving successfully commercial nuclear fusion energy, fully understanding of the interaction between plasma particles and plasma facing components is one of the essential issues. Tungsten, due to good thermal and mechanical properties such as high thermal conductivity and melting temperature, is one of the most promising candidates. However, the plasma facing components interacting with the extreme environmental conditions such as high temperature and radiation may lead to nanostructure formation, sputtering and erosion that will lead to material degradation. And these deformations may influence not only properties of plasma facing components but also might affect the plasma itself. For example, the contamination of plasma with a few amounts of tungsten, a high Z element, as a result of erosion or sputtering may cause core plasma cooling that results in loss of plasma confinement. Additionally, the retention of hydrogen isotopes, especially tritium, in tungsten is essential issue because of its radioactivity and market value.

In this study, deuterium trapping in tungsten is analyzed by molecular dynamics method and the effect of pre-irradiation on trapping is studied. Non-cumulative studies show that the increase in the energy of hydrogen isotopes rises the absorption rate, the initial implantation depth, and the average resting time for initial implantation. Additionally, the effect of implanted deuterium due to pre-irradiation on the hydrogen isotopes trapping is analyzed by combining both cumulative and non-cumulative simulations, and results indicate that while the increase in the pre-irradiation time raises the absorption rate of deuterium with higher energy than 80 eV, it causes a decrease the initial implantation depth and the average resting time for initial implantation because of deuterium-deuterium interactions. Additionally, the deuterium-deuterium interactions may transfer enough energy to implanted deuterium to start a motion which may lead to deeper implantation or escaping from the surface of tungsten. The escaping from surface as a result of deuterium-deuterium interaction could explain the decrease in accumulation rate of deuterium while absorption rate rises.

1. INTRODUCTION

The increase of the awareness of the global warming is on the rise (the Kyoto Protocol and the Paris Agreement) and some political leaders and governments implemented strict policies about using and researching alternative sustainable energy sources to produce environmentally friendly energy. Fusion energy is one of those alternative energy sources, and enormous research and development studies focus to achieving sustainable fusion energy due to the appeals of it such as essentially unlimited fuel, no production of carbon dioxide or air pollution, safety major accidents, and free from long-lived radioactive waste.

To become stable, elements on the earth may divide on small elements which is called fission or combine with other elements to produce higher elements which is called fusion. Both reactions cause the energy releasing and the energy is categorized based on its reaction such as fusion energy or fission energy. Fission energy has been harvested since the Experimental Breeder Reactor (EBR-1) was used to illuminate four light bulbs in 1951 by nuclear power plants (NPPs). According to the nuclear technology review of the International Atomic Energy Agency (IAEA) in 2019, 450 NPPs were world widely operational with total capacity of 396.4 GW(e)[1]. For fusion energy, there is no commercial power plant yet. However, there are abundance of studies focusing to achieve fusion energy for commercial use. And the majority part of these research investigates the fusion energy of deuterium and tritium to achieve commercial fusion power due to high cross section at the lower temperature compare to other potential fuel combination such us deuterium-deuterium.

For tokamak, one pioneer design type of fusion reactors, including International Thermonuclear Experimental Reactor (ITER) and Demonstration Power Station (DEMO), the deeply understanding the interaction mechanism between the plasma and the first wall is one of the most critical issues to achieve a sustainable fusion energy. The main roles of the first wall and divertor materials are to be able to withstand the extreme conditions such as high heat and high radiation, and to transmit thermal energy away from the surface. So, the design of modern fusion materials, the selection of the plasma facing materials (PFMs), and the comprehensive analysis of the interactions between plasma and the PFMs are critical to accomplish the sustainable fusion energy.

The potential candidates for PFMs are graphite, beryllium as low-Z materials and tungsten as high-Z material. The major drawback of carbon, a low-Z material with high thermal conductivity, is that carbon chemically interacts with hydrogen isotopes[2], which causes chemical sputtering. This phenomenon also creates safety and fuel resource concerns because of the production of volatile hydrocarbons, the product of carbon and tritium reactions[3][4]. For beryllium, lower erosion resistance and low melting point are the disadvantages. Lower erosion resistance generates more plasma contamination due to material transform from the first wall, and low melting point could not tolerate an increase in temperature because of the plasma disruption under high flux, high temperature plasma loading[5]. On the other hand, tungsten has higher melting point and thermal conductivity, and lower physical sputtering yield compared to other two candidates. Additionally, hydrogen isotopes do not form bond with tungsten which means no chemical sputtering [6]. The drawback of tungsten comes from its atomic number. Since it is a high-Z material, tungsten impurities in plasma cause high plasma energy losses, so the tolerance of the fusion process to amounts of tungsten in the core plasma is limited[7].

The focus of this study is the trapping of hydrogen isotopes in tungsten. Under the fusion environment, tungsten is exposed to extremely high fluence of hydrogen isotopes irradiation. Since they are highly mobile in tungsten, they will diffuse until be trapped. The accumulation of hydrogen isotopes in tungsten and bond formation of between themselves will cause the formation of blisters and bubbles[8]–[11], which cause degradation of the thermal and mechanical properties of tungsten. These blisters or bubbles can also eject tungsten dust by bursting which increases radiative losses as a result of plasma contamination with high-Z interstitials. So, to understand how hydrogen isotopes trapped in tungsten and to understand the relationship between hydrogen isotopes trapping and the formation of blisters and bubbles in tungsten are vital to accomplish the design of the PFMs for fusion reactors. In this study, molecular dynamics (MD) method is employed to examine the hydrogen isotopes trapping in tungsten by the simulation of the deuterium bombardment on tungsten.

1.1 Molecular Dynamics

Molecular Dynamics is a widely used atomistic simulation method, which has very large application areas from materials science to biochemistry. It can present details of atomistic

processes in microstructural evolution. Basically, it can be described as a method of particle tracking. Practically, the molecular dynamics method produces the trajectories of an N-particle system by employing some equations with suitable interatomic potential, initial and boundary conditions. The molecular dynamics is classified whether quantum molecular dynamics or classical molecular dynamics. If it employs Schrodinger equations, it is called quantum molecular dynamics. For classical molecular dynamics, Newton's equations of motion are operated. In our study, classical molecular dynamics method will be employed, and the equations in classical molecular dynamics are

$$m_i \frac{d^2 \boldsymbol{r_i}}{dt^2} = -\nabla_{\boldsymbol{r_i}} U(r^{3N}), i = 1, \dots, N \tag{1.1}$$

where m is the mass, **r** is the position of the i-th particle and U is potential energy on it. Once the initial conditions such as position of particles and energy distribution of the system are introduced, the classical MD method can determine the positions, velocities of particles and forces on them. Then, it numerically calculates the new positions and velocities of particles by using Taylor series expansion.

Varied classical MD codes, such as assisted model building with energy refinement (AMBER)[12], the large-scale atomic/molecular massively parallel simulator (LAMMPS)[13], and nanoscale molecular dynamics (NAMD)[14] are available. In this study, LAMMPS code is employed to analyze the hydrogen isotopes trapping in plasma facing components and how the pre-irradiation invokes the process. LAMMPS is an open source classical molecular dynamics code developed by Sandia National Laboratory. It has parallel running capability through message passing interface (MPI).

1.2 Interatomic Potential

Interatomic potential, which describes the interaction of particles in a system, is one of the essential parameters for classical molecular dynamics. The accuracy of classical molecular dynamics directly depends on how accurately the interactions between particles in the system are determined. So, selecting suitable interatomic potential is crucial to achieve desired outcomes. However, pair potentials [15]–[19], many-body central force potentials [20]–[28] and its empirical modification [29], bond order potentials [30]–[34], modified embedded atom method potentials[35], [36] and

fourth moment tight binding potentials [23], [37], [38] are some different form of interatomic potential, which are accessible in the literature. Each of potential has its own advantages and disadvantages, so it is critical to choose the interatomic potential carefully and to check its accuracy. In this study, analytical bond-order potential (ABOP) describing the atom binding states is employed. This form of potentials can represent the chemical bonding interaction with rational accuracy. Yang and Hassanein, in their research[9], point out a comparison of the W-H potential developed by Li et al.[34] and W-C-H potential developed by Juslin et al.[30]. In addition to underestimation of tungsten melting point, ABOP developed by Juslin et al.[30] produces point defect parameters less accurately. However, ABOP developed by Li et al.[34] not only overestimates the tungsten melting point but also its runtime is 3 or 4 times greater because of long cutoff parameter. Additionally, Li's values were not replicated by the interstitial properties, so the W-H potential parameters might be incorrect. Under these circumstances, interaction between deuterium and tungsten in this study is represented by employing the ABOP developed by Juslin.

1.3 Deuterium on Tungsten

Experimental studies focusing on tungsten bombarded by low energy, high flux hydrogen isotopes show that hydrogen isotopes can cause surface modification such as pinhole, blister and bubble even if their energy is much lower than threshold energy to displace a tungsten atom in lattice[8], [10], [11], [39]–[43]. The subsurface deuterium bubble formation in tungsten under the low energy high flux deuterium plasma irradiation was investigated by Y.Z. Jia et al[40]. In the subsurface region, Y.Z. Jia et al. observed the uniformly distributed bubbles caused by deuterium super saturation state (figure 1-1(b) and (d)). In the study, tungsten samples at 500 K or 1000 K were exposed to deuterium plasma with 38 eV energy. The peak of the deuterium flux was 1.5×10^{24} $m^{-2}s^{-1}$ and total fluence of deuterium on each sample was fixed to 6×10^{26} m^{-2}. Scanning electron microscope (SEM) and transmission electron microscope (TEM) were used to observe the surface morphology of tungsten and deuterium bubbles in the near surface region, respectively. The SEM and TEM image of surface morphology and cross-section morphology of tungsten surfaces after exposure to low energy high flux deuterium plasma at 500 K were displayed in figure 1-1. While the blisters and ordered surface nano-structures were observed on [111] surface in figure 1-1 (a), flakings and pinholes were detected on [001] surface in figure 1-1 (c) instead of blisters and ordered nano-structures. The cross-section morphology corresponding figures 1-1 (a) and (c) were

showed in figures 1-1 (b) and (d), respectively. Homogenously distributed bubbles indicated by white arrows in figures were observed in the surface region. On [001] surface, the bursting of deuterium bubble caused flaking of the surface and generated pinholes on the tungsten surface. However, blistering on the tungsten surface were generated by deuterium bubbles on [111] surface. When the experiment repeated at 1000 K, the depth of bubbles where they are formed became greater than at 500 K because of the enhanced diffusion, and the size of bubbles were smaller. Although bubbles were formed at 1000K, the blistering were not induced by bubbles due to deeper position and smaller size, which matched with the literature. Another research focusing surface blistering on tungsten exposed to high flux deuterium was done by H.Y. Xu et al[42]. Tungsten samples at the temperature range from 423 K to 873 K were exposed to high flux (1-2 x 10^{24} $m^{-2}s^{-1}$) deuterium with 38 eV up to fluence 7 x 10^{26} m^{-2}. In their study, not only relatively small size of surface blistering was observed even at the low fluence 0.2 x 10^{26} m^{-2} but also the blistering showed

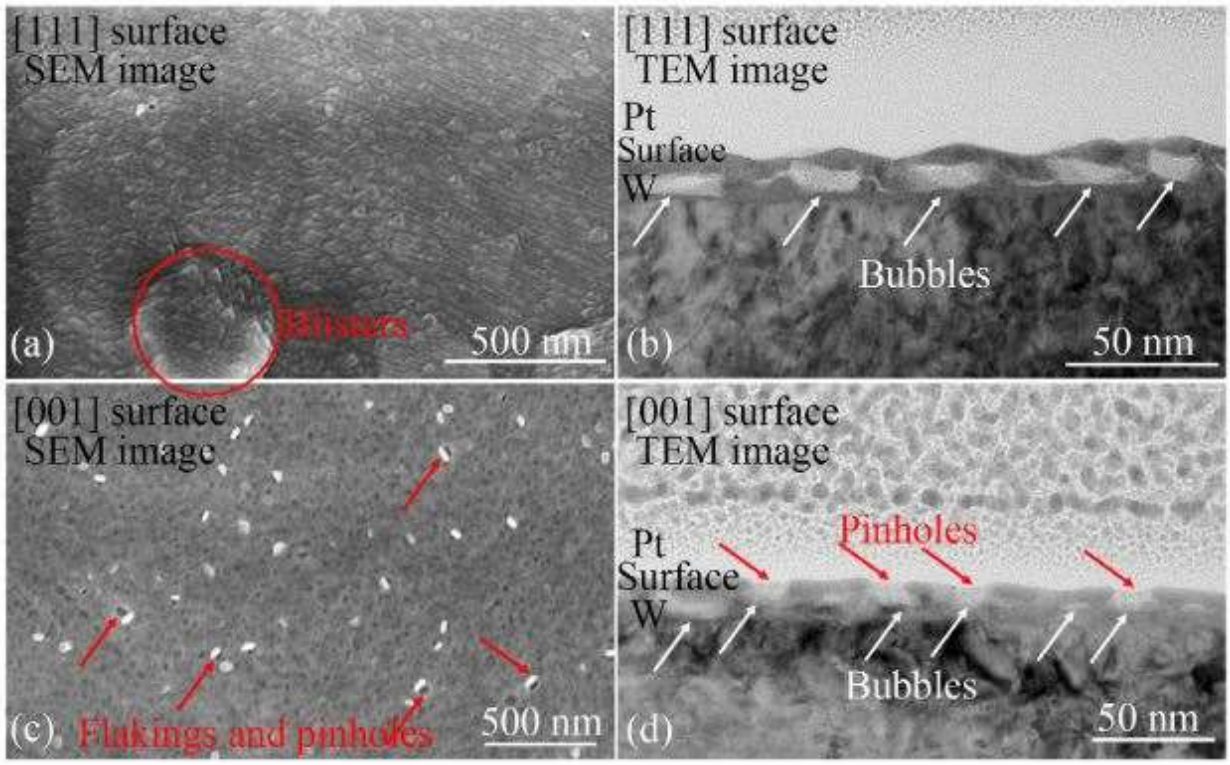

Figure 1-1 Morphology of W sample exposed to D plasma at 500 K. (a)(b) surface and cross-section morphology of [111] surface, (c)(d) surface and cross-section morphology of [001] surface. (Adopted from [40]).

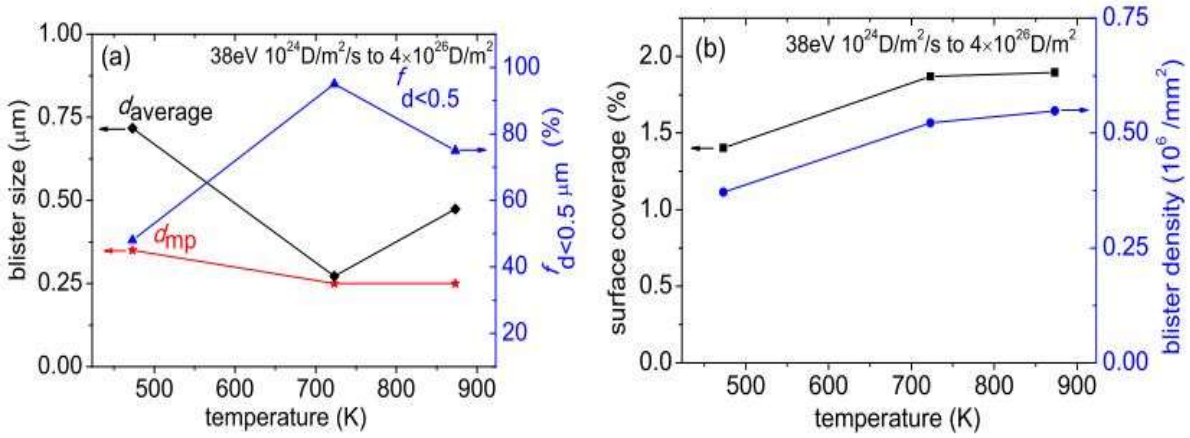

Figure 1-2 Statistical evaluation of (a) the average diameter, most popular diameter of blisters, and the fraction of blisters with size less than 0.5 μm, (b) the surface coverage and the number density of blisters after exposed to deuterium (38 eV) plasma with fluence of 4 x 10^{26} cm^{-2} (Adopted from [42]).

persistence at high temperature. Figure 1-2 displayed the plot of statistical evaluation of blister parameters corresponding to surface temperature. The average diameter of blister was denoted by $d_{average}$, d_{mp} referred the most popular diameter, and $f_{d<0.5}$ designated the fraction of blistering having smaller diameter than 0.5 μm. As seen in figure 1-2, even though the most popular diameter of blistering declined, both the surface coverage of blisters and blister density increased with the rise of the surface temperature.

2. MOLECULAR DYNAMICS SIMULATION OF DEUTERIUM-TUNGSTEN SYSTEM

This chapter is organized as follows. Subsection 1 explains the conversation of interatomic potential from ABOP to Tersoff potential. Subsection 2 describes the creation of tungsten substrate for further simulation. Subsection 3 and 4 illustrate the non-cumulative and cumulative bombardment of deuterium, respectively. LAMMPS, Ovito and Origin are the adopted tools for this study. Details are discussed in further parts.

2.1 H-W Interatomic Potential

In LAMMPS, the interatomic potential in the form of ABOP cannot be directly employed. However, Tersoff potential defining three-body interaction, one of the implantable interatomic potentials in LAMMPS, can be obtained from ABOP. In Tersoff potential, the center atom i, in the many body system, is bonded to the second atom j and the third atom k influencing the bond between atom i and atom j. Xue and Hassanein studying the molecular dynamics simulation of deuterium trapping and bubble formation in tungsten[9] converted the deuterium-tungsten interatomic potential from ABOP to Tersoff potential by using following formulation:

$$
\begin{aligned}
m^{LAM} &= n^{LAM} = 1 \\
\beta^{LAM} &= \omega \\
\lambda_1^{LAM} &= \beta\sqrt{2S} \\
\lambda_2^{LAM} &= \beta\sqrt{\frac{2}{s}} \\
\lambda_3^{LAM} &= \alpha_{ijk} \\
(cos\theta_0)^{LAM} &= -h \\
A^{LAM} &= \frac{D_0}{S-1} e^{\lambda_1^{LAM} r_0} \\
B^{LAM} &= \frac{SD_0}{S-1} e^{\lambda_2^{LAM} r_0} \\
R^{LAM}, D^{LAM}, c^{LAM}, d^{LAM}, \gamma^{LAM} &= R, D, c, d, \gamma
\end{aligned}
\tag{2.1}
$$

where the ABOP coefficients from Juslin's research paper[30] are used to calculate the Tersoff potential variables donated by LAM superscript. More detailed information about transformation interatomic potential can be found Xue's study[9]. The full list of Tersoff potential variables for hydrogen-tungsten system can be found in Appendix 1.

2.2 Creation of Tungsten Substrate

Body centered cubic (BCC) structure of tungsten with lattice constant of 3.165 Å, which makes the potential energy minimum based on the BCC tungsten energy minimization calculation, is used to create the tungsten substrate. The substrate consists of 8000 W atoms. The dimension of simulation box is 25.34x25.34x280 Å. X- and y-directions are set to periodic boundary conditions, which allows that atoms leaving the system from one side of box reenter the system from other side. Z-direction, however, is non-periodic and fixed. If an atom leaves the simulation box from one side of z-direction, it will be deleted. The bottom layers of tungsten atoms in 10 Å are fixed, which means initial velocities of these atoms and the force on them are set to zero. Tersoff potential is used to determine the interatomic potentials and initial velocity of W atoms is distributed by a Gaussian distribution based on the substrate temperature. The chosen time step and step number for relaxation are 0.01 ps and 6000, respectively. This time is required to achieve thermal equilibrium, to minimize the potential energy of the substrate, and to have more realistic energy distribution of tungsten atoms. Figure 2.1 shows the tungsten substrate at 1000 K after 60 ps rescaling time. While the perspective view of full W substrate is presented in figure 2-1 (a), only the surface region of the simulation domain is showed in figure 2-1 (b) to highlight the surface structure of the tungsten substrate. A sample of LAMMMPS code of substrate tungsten creation is in Appendix 2.

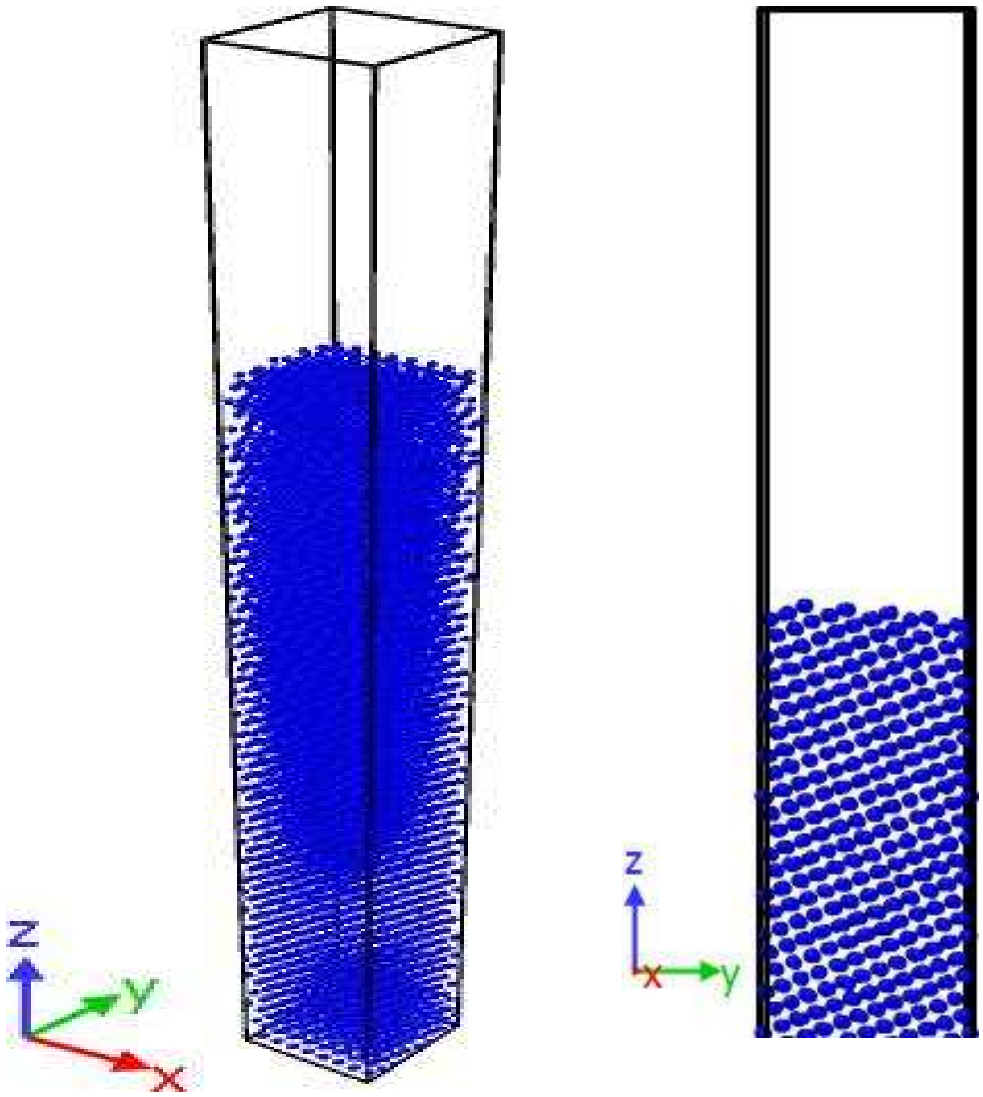

(a) Perspective view of full simulation box after rescaling

(b) Ortho view of the surface region of simulation box

Figure 2-1 Simulation box of W substrate at 1000K after 60 ps rescaling

2.3 Non-Cumulative Bombardment

Non-cumulative bombardment type of simulation is used to study the angle dependence of deuterium-tungsten system, the effect of deuterium energy and substrate temperature on deuterium trapping in W substrate, and the effect of pre-irradiation on the trapping of hydrogen isotopes. In this type of simulation, a substrate is bombarded by a single particle and this particle is tacked until it leaves the simulation box, or its kinetic energy reduces under a certain value. And then, the

information is saved, and the process is started again with a new particle. This repeating continues until the number of simulation particle reaches a certain value to be able to deduce the statistically essential information from outcomes.

In our non-cumulative simulation, the W substrate at various temperatures ranging from 300 K to 1000 K is bombarded by 10-100 eV deuterium atoms. The Berendsen thermostat[44] is used to keep the atoms in Berendsen region at the desired temperature. Figure 2.2 demonstrates the configuration of Berendsen region. The region covers the atoms located in 3.165 Å thick from each side and 12.66 Å thick from the fixed atoms at the bottom. Deuterium is located at 15 Å above the W surface randomly and it heads toward to the W surface with various angle ranging from zero to 80-degree respect to surface normal. Time step of simulation is set to 0.5 fs. After each 50 steps, the position and kinetic energy of deuterium are checked and requirement for another 50 steps is determined. If deuterium is still in the simulation box and its kinetic energy is higher than 0.5 eV, simulations continue another 50 steps. The same process is repeating as far as total step number is lower than maximum step number and deuterium with higher energy than 0.5 eV is still in the system. When deuterium leaves the simulation box or its kinetic energy reduces under 0.5 eV or

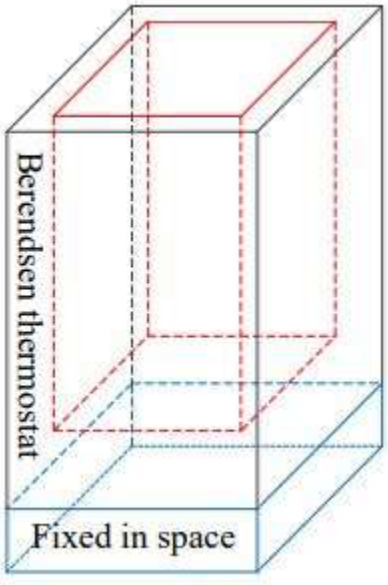

Figure 2-2 Berendsen region configuration. Blue region shows the fixed atoms in space, and the temperature of atoms from outside of red box to each simulation side and above the fixed regime are controlled by Berendsen thermostat.

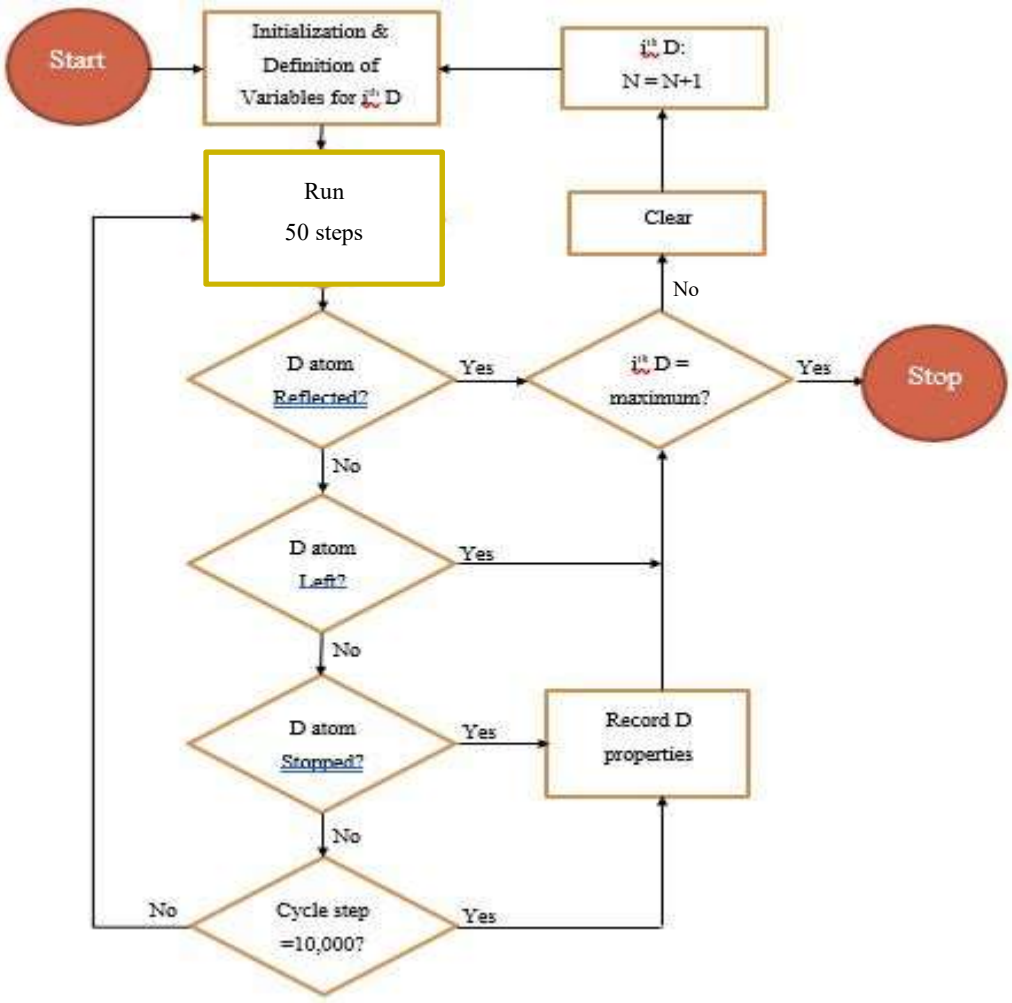

Figure 2-3 Non-cumulative bombardment flowchart

the step number reaches its maximum number, the simulation is stopped and the outcome of it is recorded. If deuterium is still in the simulation box, it will be deleted after recording its position and kinetic energy. Then, new deuterium is replaced as previous ones and the whole process starts again. The flow chart of non-cumulative bombardment is illustrated in figure 2.3. This procedure continues until the total number of deuterium atoms hits a desired number. A sample LAMMPS script for non-cumulative bombardment can be found in Appendix 3.

2.4 Cumulative Bombardment

Cumulative bombardment type of simulation is employed to analyze the effect of pre-irradiation on deuterium trapping in W substrate, to observe the effect of the deuterium-deuterium interaction

on trapping mechanism, and to study the structure modification caused by implanted deuterium. In this type of simulation, a substrate is periodically bombarded by particles, the particle is deuterium atom in our case, until the total number of particles reaches the desired value.

In our cumulative simulation, the W substrate at 1000 K is bombarded by 100 eV deuterium atoms. The Berendsen thermostat keeps the atoms in Berendsen region at the desired temperature. The region covers the atoms located in 3.165 Å thick from each side and 12.66 Å thick from the fixed atoms at the bottom. Initial position of each incident deuterium atom increases from 15 Å to 40 Å in case of swelling. X and y coordinates of initial deuterium are selected randomly, and the deuterium atoms toward to W substrate perpendicularly. The step size of the simulation is set to 0.5 fs and at the end of every 5,000 steps, a new deuterium atom enters the system from its initial position. Figure 2-4 shows the flowchart of cumulative bombardment. A sample LAMMPS script can be found in Appendix 4 for cumulative bombardment.

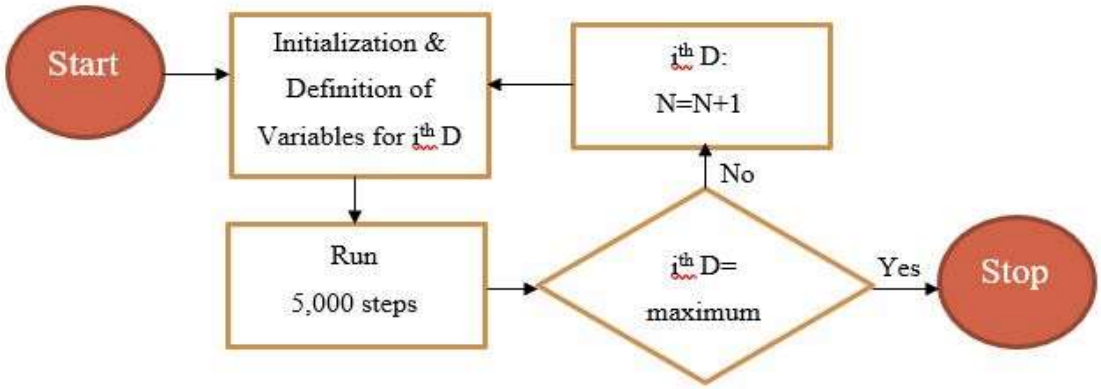

Figure 2-4 Cumulative bombardment flowchart

3. RESULTS

The absorption rate, the reflection rate, the sticking coefficient, the average deuterium resting time, the average initial implantation depth, the deuterium implantation profile and the pace of the deuterium cumulation are studied by using non-cumulative simulation, cumulative simulation or combination of them to investigate deuterium trapping on tungsten. The dependence of hydrogen isotopes trapping on the parameters such the effect of the angle and the energy of incident particle, the effect of the temperature, and the effect of the pre-irradiation, is analyzed. The results chapter is organized as follows: angle dependence, energy and temperature dependence, and the effect of pre-irradiation.

3.1 Angle Dependence

Absorption rate is one of the essential parameters in investigating the deuterium trapping in W. It describes the initially absorbed deuterium atoms in W substrate in terms of percentage, and it is defined as the total number of absorbed deuterium atoms in the W substrate per the total number of deuterium using for bombardment.

The angle dependence of deuterium trapping is examined by non-cumulative type simulation. The tungsten substrate at 600 K is bombarded by 80 eV deuterium atoms. The size of simulation box is 25.34 X 25.34 X 280 Å and deuterium atoms are located 15 Å above the surface of W and its x- and y-coordination are selected randomly. The angle of incident particle respect to surface normal varies from 0- to 80-degree. Totally, 3000 deuterium atoms are simulated. Figure 3-1 demonstrates the angle dependence of absorption rate and reflection rate. As seen in the figure 3-1(a), absorption rate shows a slight increase between zero to 30-degree respect to the surface normal, then it sharply decreases from around 0.4 to lower than 0.05. It clearly states when the angle of low energy incidence deuterium is high, it is more likely to be reflected from the surface instead of being trapped in tungsten substrate. For reflection rate, exactly opposite trend is observed. Figure 3-1(b) presents the angle dependence of reflection rate of incident deuterium atoms. Similar behavior is also detected for graphene-hydrogen system. Saito and his colleagues examine the angle dependence of reaction between graphene and hydrogen atom using molecular dynamics

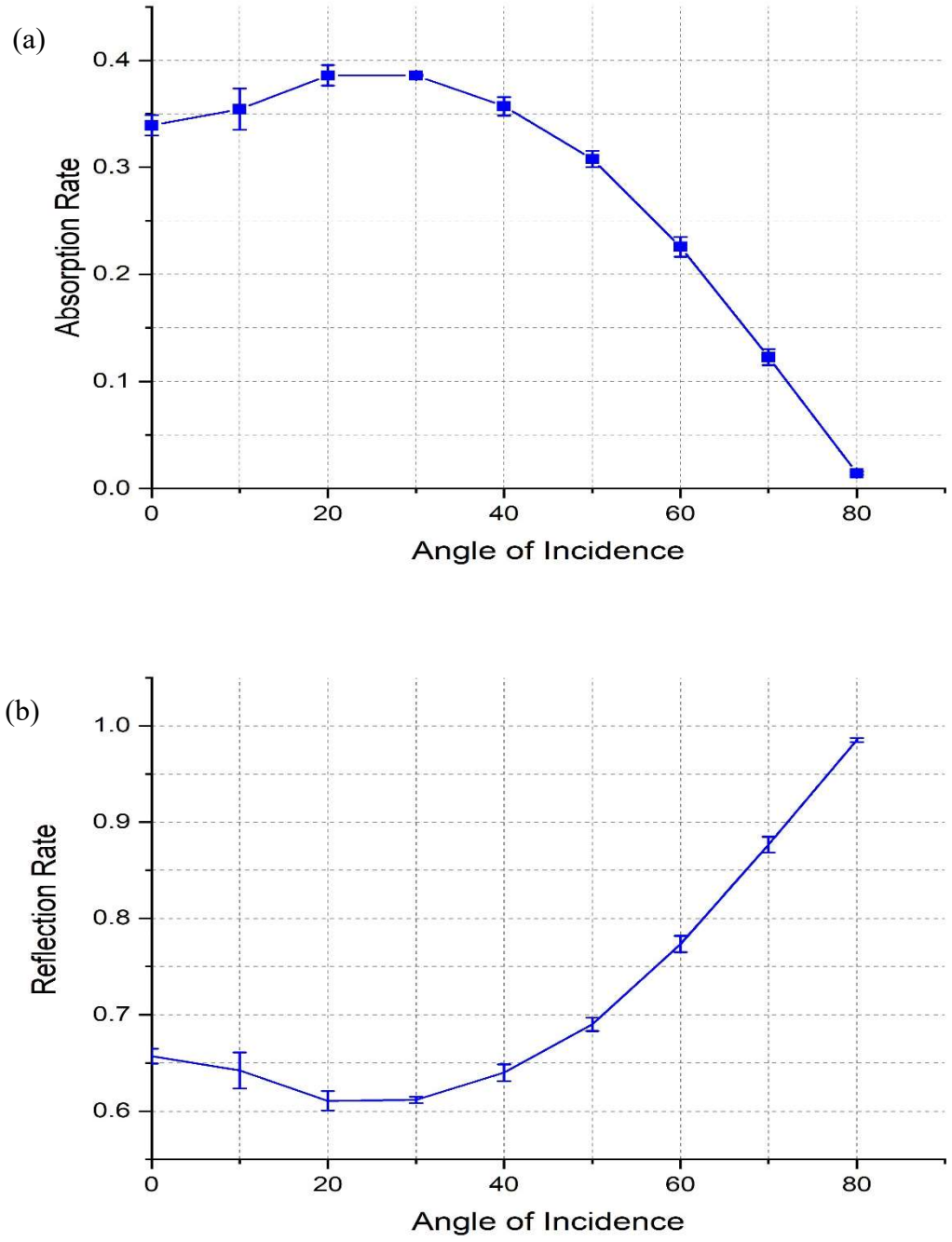

Figure 3-1 Angle dependence of absorption rate (a) and reflection rate (b) of deuterium with 80 eV on tungsten substrate at 600 K

simulation[45]. They found out that the reflection rate and penetration rate showed angle dependence and the penetration rate increased slightly when the angle increased from zero- to 20-

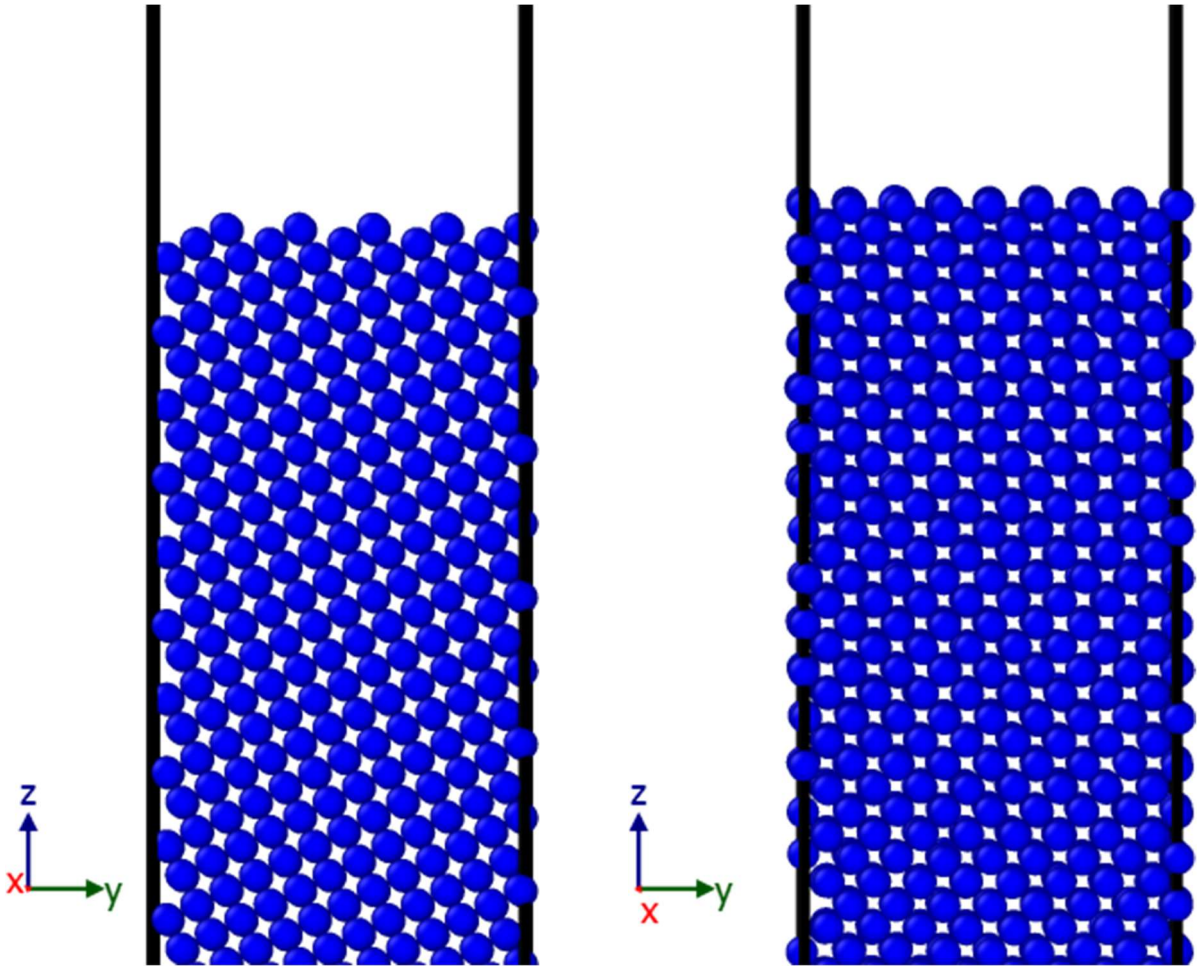

(a) Surface structure of PCW substrate (b) Surface structure of SCW substrate

Figure 3-2 Side view of the different surface structure of W substrate at 600 K

degree respect to surface normal. It looks like that 30-degree angle respect to surface normal is preferential for our deuterium-tungsten system. When deuterium atoms toward to the surface with 30-degree respect to surface normal, they most likely penetrate the surface of W and are initially implanted in tungsten substrate compare to other angles. To understand the relationship between preferential angle and surface structure, two tungsten substrates with different surface structure are studied. Poly-crystalline tungsten (PCW) and single-crystalline tungsten (SCW) simulation domains are created at 600 K temperature and illustrated in figure 3-2. As seen in Figure 3-3, the surface structure does not only change the preferential angle, but also it increases the number of preferential angles. While there is one preferential angle around 30-degree for PCW substrate, two preferential angles are observed around 5- and 45-degree for SCW substrate.

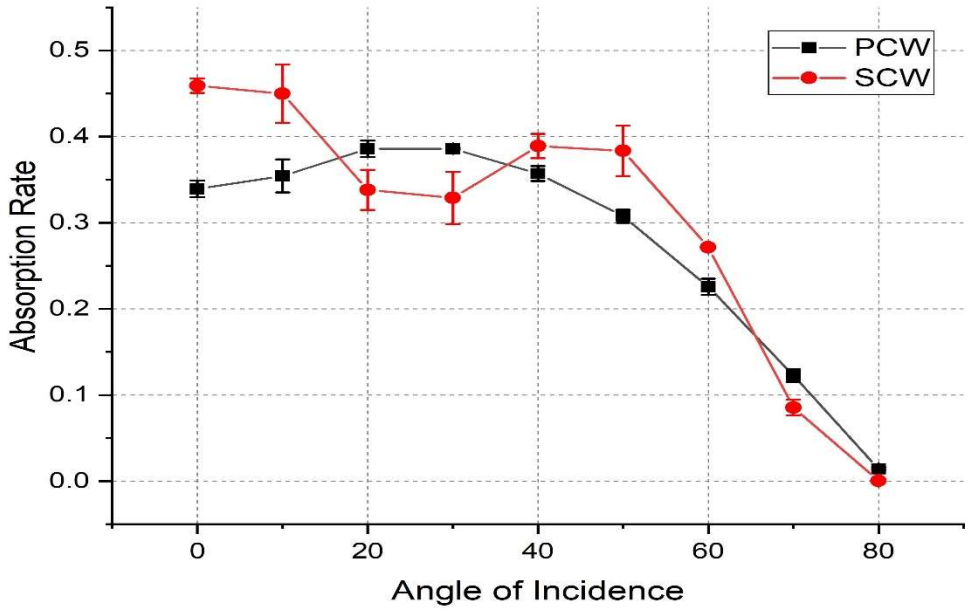

Figure 3-3 Angle dependence of absorption rate of deuterium with 80 eV for different type of surface structure at 600 K

3.2 Energy and Temperature Dependence

The effects of the deuterium energy and the substrate temperature on deuterium trapping in tungsten are investigated by non-cumulative type of molecular dynamics simulation. Tungsten substrate at the temperature ranging from 300 K to 1000 K is bombarded by deuterium atoms with various energy between 10 eV and 100 eV. The simulation box is created from 0 to 25.34 Å in x- and y-direction and from -200 Å to 80 Å in z-direction. The region between 0 to -200 Å in z-direction is filled with deuterium atoms. After rescaling the substrate temperature, Berendsen thermostat is used to maintain the atoms in Berendsen region at the desired temperature during the simulations. Initial x and y coordinates of energetic deuterium are selected randomly, and it is located at 15 Å above the surface of the tungsten substrate. Then, the tungsten substrate at the various temperature is bombarded perpendicularly by deuterium atoms with various energies. In each case, 3 sets of 1000 deuterium atoms are employed to investigate the effect of the deuterium energy and the substrate temperature on deuterium trapping. Figure 3-4 displays the dependence

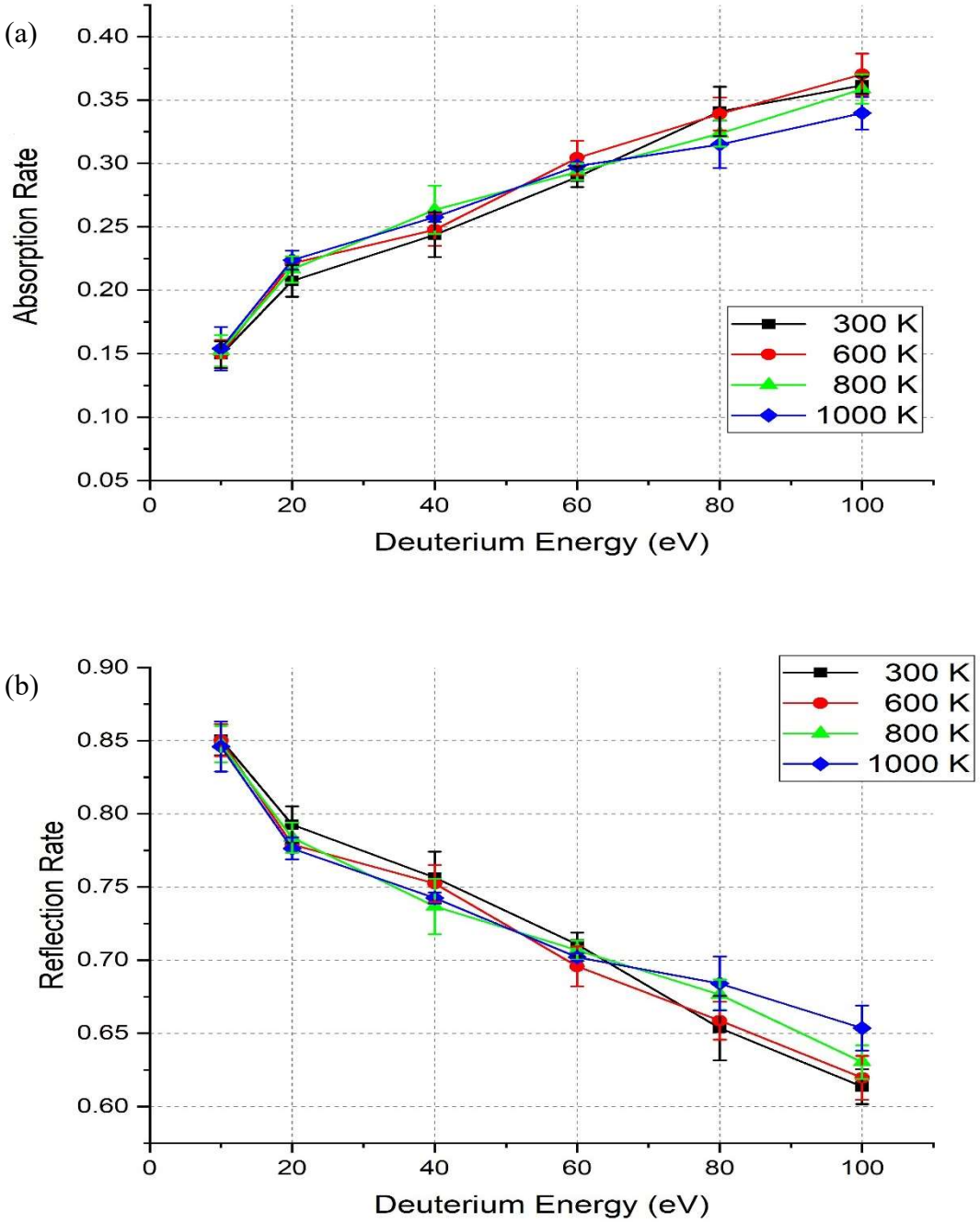

Figure 3-4 Absorption rate (a) and reflection rate (b) for various tungsten substrate temperatures and deuterium energies

of absorption rate and reflection rate on the deuterium energy and tungsten substrate temperature. While the absorption rate of deuterium in tungsten increases while the energy of deuterium raises,

the reflection rate shows an opposite trend. The reason for that, the probability of penetration at the tungsten surface becomes higher as the energy of deuterium increases, so much more deuterium atoms penetrate the surface of the tungsten substrate instead of being reflected or sticking in the tungsten surface region and escaping from there. In the study of temperature effect, two different trends can be observed. In the case of deuterium with energy higher than 50 eV, the increase in temperature causes a slight decrease in the absorption rate except some variation for 300 K and 600 K temperature where the absorption rate rises. In other words, even though much more deuterium atoms tend to be reflected from tungsten substrate at 600 K compare to W substrate at 300K, the absorption rate for tungsten at 600 K is higher than the absorption rate for 300 K. It is important to remember that our simulation ignore the deuterium atoms leaving the simulation box from bottom side as a result of channeling effect, and these atoms are neither trapped in W substrate nor reflected from the W substrate. In the study done by Alimov and Roth[46], similar trend was also observed. They examined the effect of the substrate temperature on the deuterium retention in SCW and PCW. For both structures of W, the retention profile shows similar trend; it rises with temperature until passing some point then it starts declining. For the lower deuterium energy part, the absorption rate shows opposite trend compare to the higher deuterium region. To analyze this

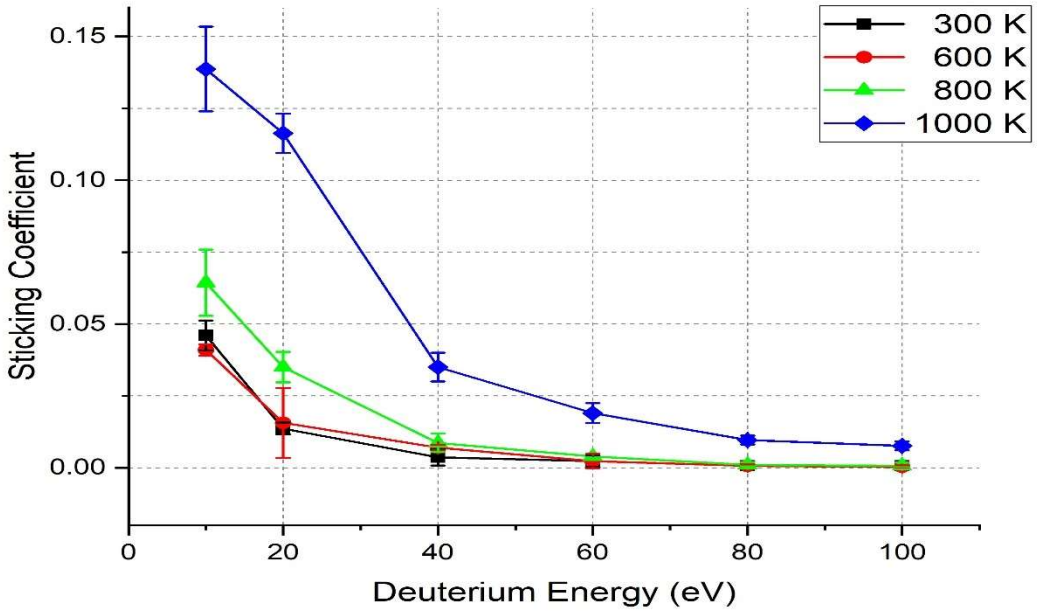

Figure 3-5 Sticking coefficient for various tungsten substrate temperatures and deuterium energies

part, the sticking coefficient of the deuterium on W surface should be examined. It is defined as the reaction probability, i.e. the reactivity of a single deuterium atom with a reactive site on the W surface and it is assumed to roughly equal the ratio of the number of deuterium trapping in surface region over the total incident deuterium in this study. Figure 3-5 illustrates the energy dependence of the sticking coefficient for various tungsten temperatures. As seen in the figure 3-5, the sticking coefficient increases when the substrate temperature rises while it eases with increasing in deuterium energy. Similar behavior of sticking coefficient was also observed by Yang and Hassanein[9]. Especially, at the low energy region, the increase in the sticking coefficient while the temperature rising grows faster. This difference could explain why the absorption rate at the low energy deuterium region shows different behavior than the other region. Increase in substrate temperature make the sticking coefficient greater, and retention rate of deuterium with low energy is dominated by the sticking coefficient.

Additionally, the effect of deuterium energy and W substrate temperature on average stopping time and average implantation depth were studied, and presented in figure 3-6 and 3-7, respectively.

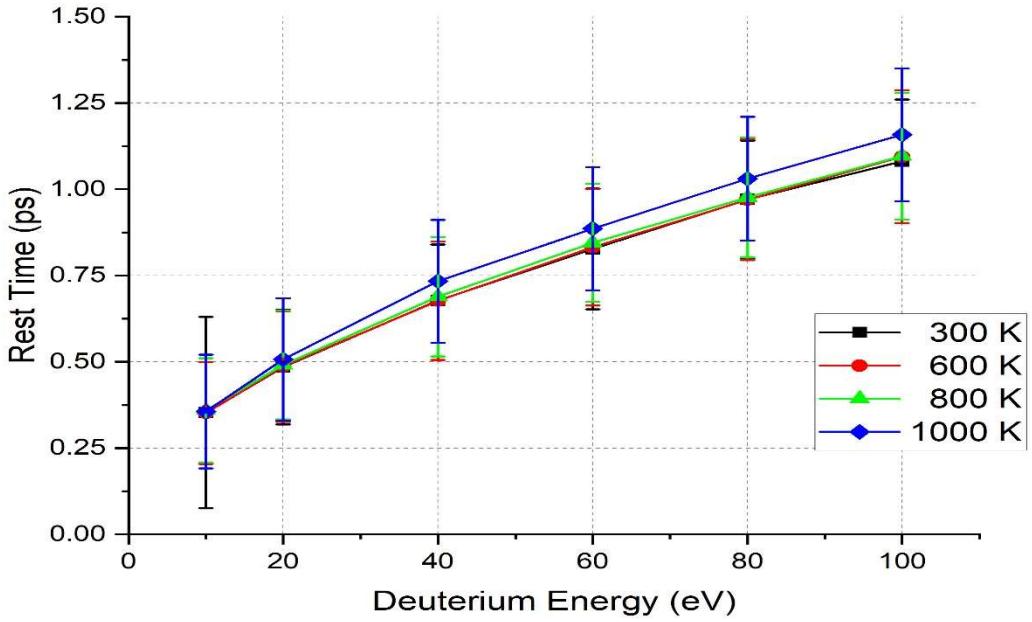

Figure 3-6 Average required time to rest for various tungsten substrate temperatures and deuterium energies

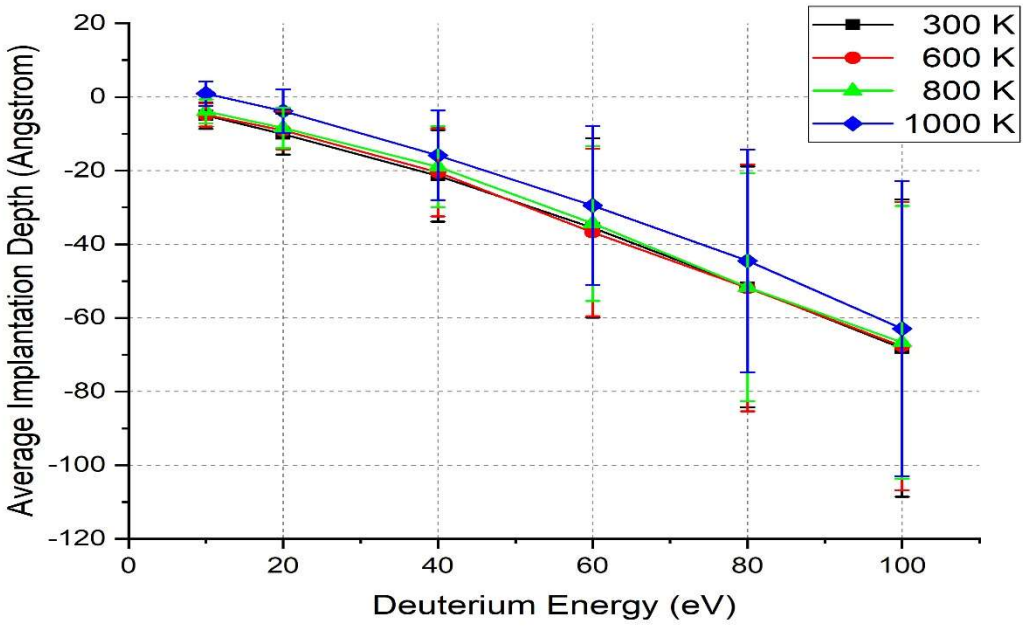

Figure 3-7 Average implantation depth of deuterium for various tungsten substrate temperatures and deuterium energies.

Figure 3-6 demonstrates the average required time to rest for a deuterium atom with various energy in the tungsten at different temperature. As the deuterium energy builds up, it requires much more interaction to lean, which boosts the average required time. Additionally, for the tungsten substrate at 1000 K, the required time to rest rises compare to others. When the temperature of substrate raises, the energy deuterium loss per interaction becomes relatively lower and the average time to rest increases. It should be noted that the average required time to rest is overestimated in non-cumulative simulations because only interaction between deuterium and tungsten is considered. In real case, deuterium atoms can interact with other deuterium atoms. So, deuterium can come to rest earlier as a result of interaction between similar mass particles which boosts the energy losses. In figure 3-7, similar temperature dependence also observed for average implantation depth. Higher energy deuterium atoms reach deeper part of W substrate and temperature barely effects the average implantation depth except the W substrate at 1000 K. Majority of deuterium is implanted around the surface for deuterium atoms with 10 eV and the week bond between tungsten and deuterium atoms makes deuterium atoms stick to the surface. Furthermore, this study only

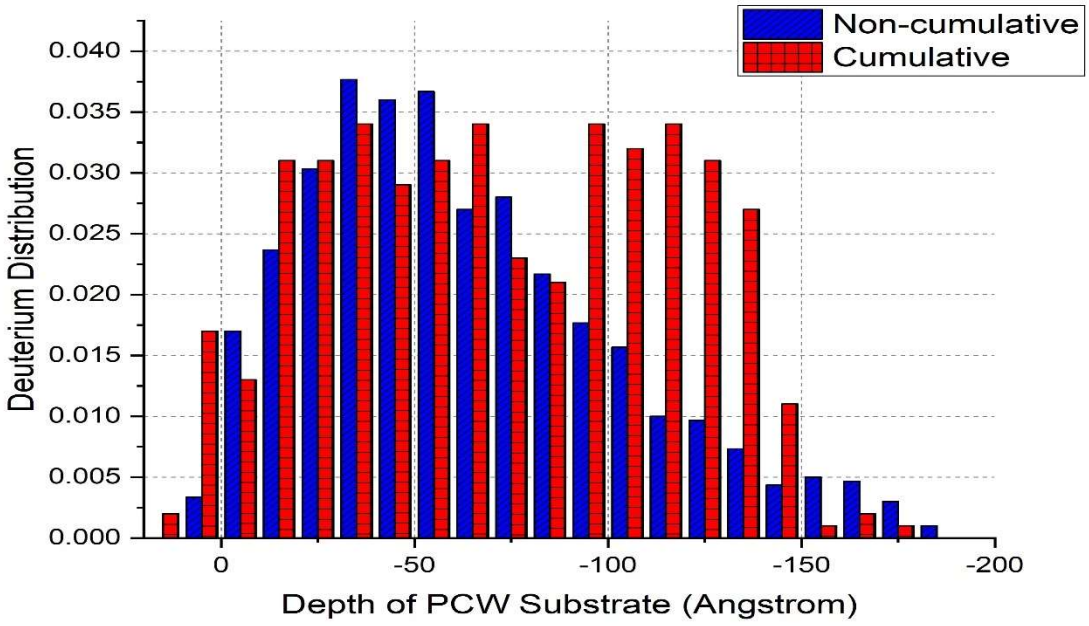

Figure 3-8 The depth profile of deuterium with 100 eV in PCW substrate at 1000 K for nun-cumulative and cumulative simulation

examines the initial rest position of deuterium atoms. When the deuterium atoms are trapped, they are removed from simulation after recording of outputs. In a realistic case, however, deuterium atom retained in W substrate can be pushed deeper as a result of collision with other deuterium atoms. Figure 3-8 shows the implantation profile of deuterium atoms for non-cumulative and cumulative simulation. As seen in figure 3-8, while majority of deuterium atoms in non-cumulative bombardment is located around -45 Å, for cumulative bombardment location of majority peak is shifted deeper side of the W substrate around -120 Å. More detailed study of deuterium-deuterium interaction is analyzed in subchapter 3.3.

3.3 The Effect of Pre-Irradiation

The effect of implanted deuterium on deuterium trapping in tungsten as a result of pre-irradiation is studied by using both cumulative bombardment and non-cumulative bombardment. The substrate tungsten samples thermalized for 60 ps at 1000 K are pre-irradiated by 100 eV deuterium during 2.5, 5.0 and 7.5 ns, respectively. The restart files including the implanted deuterium

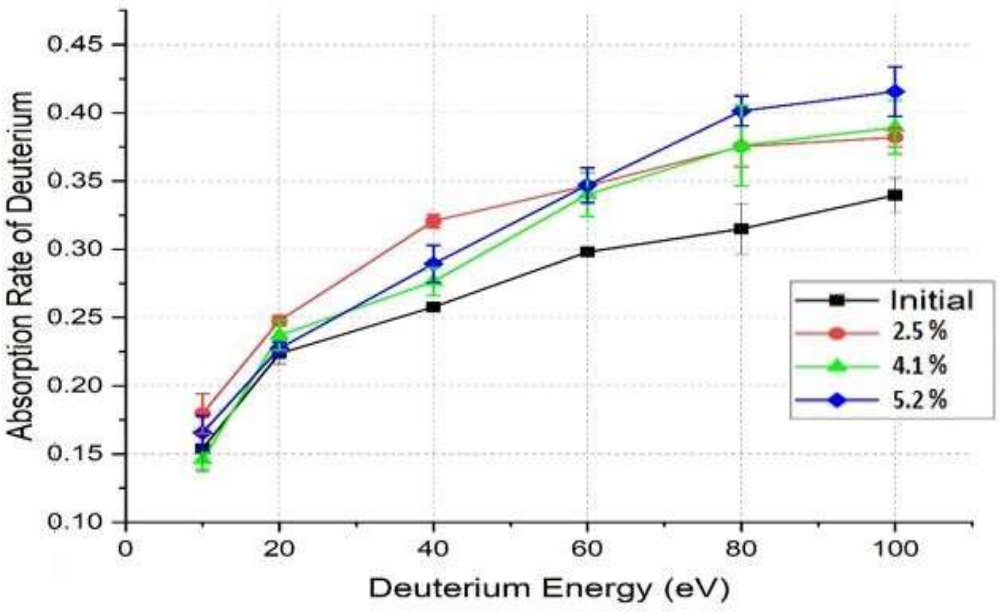

Figure 3-9 The energy dependence of the absorption rate of deuterium in tungsten substrate at 1000 K for various pre-irradiation time

energies and positions are created after each pre-irradiation. Each created file includes the different concentration ratio of deuterium and it increases with time. The deuterium concentrations in the tungsten substrate are 2.5, 4.1, and 5.2 percents for 2.5 ns, 5.0 ns, and 7.5 ns pre-irradiation time, respectively. Then, these restart files are used as substrate tungsten configurations including deuterium particles, and these substrate tungsten configurations are bombarded by deuterium with various energies (10 eV-100 eV) to analyze how the absorption rate, average initial implantation depth, and average resting time are influenced by implanted deuterium in the sample. Figure 3-9 shows the effect of implanted deuterium on the absorption rate. As seen in figure 3-9, absorption rate of deuterium in tungsten substrate with implanted deuterium is greater than the absorption rate of deuterium in tungsten only substrate, which indicates that the deuterium reflectivity rate may decrease and the number of deuterium trapping in tungsten might rise in time, which could cause the deuterium bubble formation because of the supersaturation of deuterium. Figures 3-10 and 3-11 present the average initial implantation depth of deuterium and the average required time for incident deuterium to rest, respectively. Figure 3-10 shows that the incident deuterium is initially

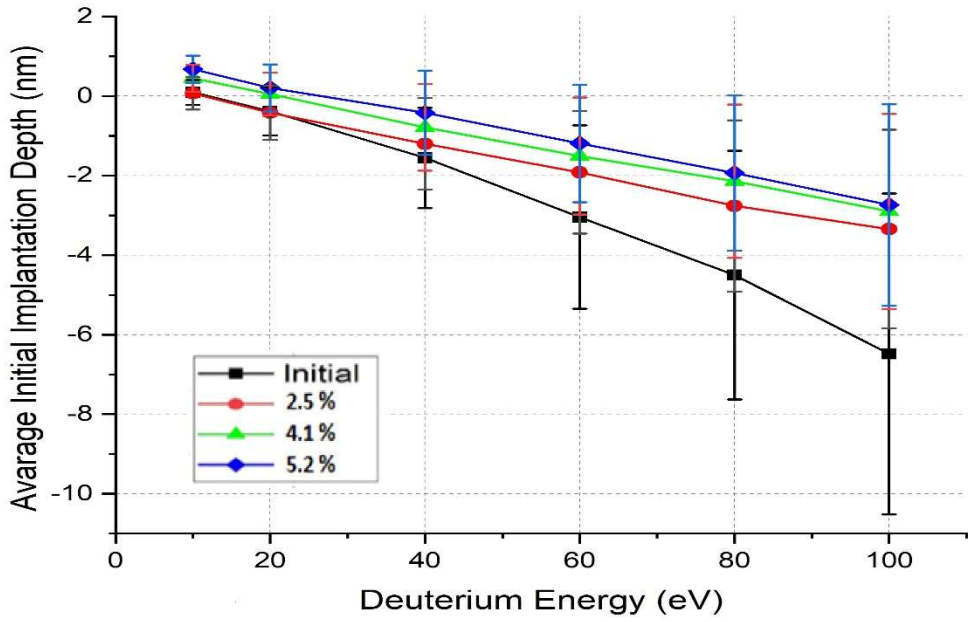

Figure 3-10 The energy dependence of the average initial implantation depth of deuterium in tungsten substrate at 1000 K for various pre-irradiation time

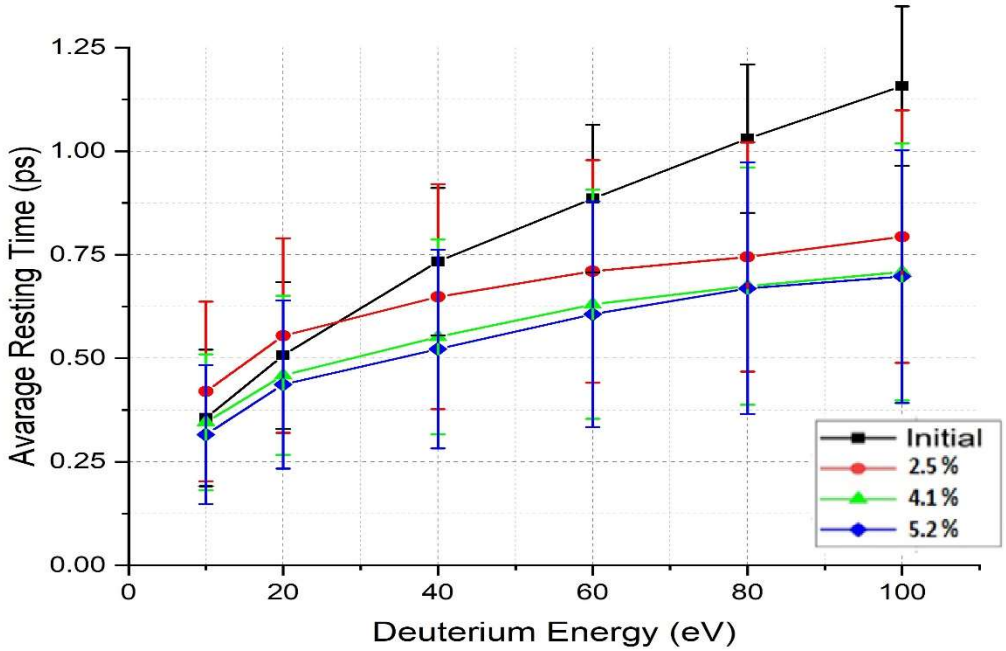

Figure 3-11 The energy dependence of the average resting time of deuterium in tungsten substrate at 1000 K for various pre-irradiation time

implanted closer to the surface while the number of implanted deuterium rising. One of the possible reasons for this behavior could be that the incident deuterium may lose its energy faster because of deuterium-deuterium interaction as indicated in figure 3-11, and deuterium may not be able to penetrate deeper because of the lack of the energy. Moreover, in figure 3-11, for the deuterium with energies from 10 eV to 30 eV, a small increase in resting time is observed from initial time to 2.5 ns while the required average time to rest decreases with implanted deuterium in all other cases. The reason for that could be the energy increase in tungsten atoms in surface region due to deuterium bombardment. The implanted deuterium atoms transfer their energy to lattice tungsten atoms, which cause a decrease the energy loss of incident particle per collision. In that case, incident particle requires much more collision to rest which explains the rise in figure 3-11 for 2.5 % deuterium concentration line.

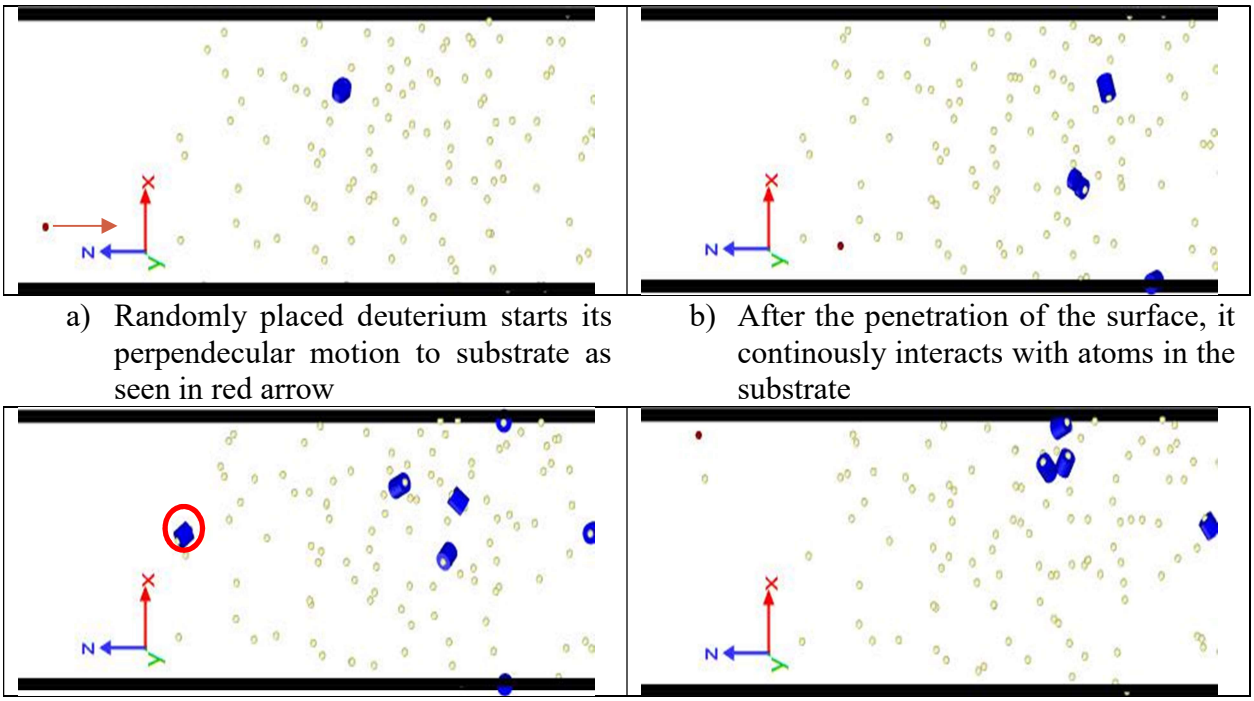

a) Randomly placed deuterium starts its perpendecular motion to substrate as seen in red arrow

b) After the penetration of the surface, it continously interacts with atoms in the substrate

c) It reaches an implanted deuterium and transfers enough energy to leave from the surface

d) It leaves the substrate from the surface.

Figure 3-12 Time evolution of the one of non-cumulative simulations. Red atom is incoming deuterium, white atoms are implanted deuterium atoms and blue shows the at least two deuterium atoms close enough to transfer the energy

For the estimation of the probability of the interaction between incoming deuterium and implanted deuterium, various number of nun-cumulative simulations are analyzed. In these simulations, the tungsten substrate with various deuterium concentration are bombarded by 40 and 100 eV deuterium atoms. Figure 3-12 shows one of these nun-cumulative simulations. In this simulation, tungsten substrate with 4.1 percent deuterium concentration is bombarded by 40 eV deuterium. The incoming deuterium is tracked, and its position is recorded for every step to analyze whether it reaches to an implanted deuterium atom enough (2.12 Å based on the article written by Zhou et al.[47]) to transfer the energy or not. As seen in figure 3-12, not only the incoming deuterium transfers its energy to implanted deuterium, but also the implanted deuterium gains enough energy to start motion which ends leaving the substrate from the surface. The probability of deuterium - deuterium interaction is calculated by dividing the number of deuterium interacting with implanted deuterium by the total number of simulations. Table 3-1 presents the probability of the interaction between the incoming deuterium and implanted deuterium based on the incoming deuterium energy and deuterium concentration in the tungsten substrate. As seen in the table, the probability of interaction between incoming deuterium and implanted deuterium is higher than 0.5 even at the lowest concentration and the lowest deuterium energy. In other words, the incoming deuterium most likely interacts with implanted deuterium atom and transfer some part of its energy to implanted deuterium. The probability of deuterium-deuterium interaction rises when the concentration of deuterium in the tungsten substrate or the energy of the incoming deuterium increases. With the increase in the concentration of deuterium during deuterium bombardment, the probability of interaction between incident deuterium and implanted deuterium will rise. And, the behavior of incoming deuterium will be influenced by the existence of implanted deuterium and its concentration.

Table 3-1 The probability of the interaction between incident and implanted deuterium

D-concentration (%) / D-energy (eV)	2.5	5.2
40	0.55	0.66
100	0.76	0.80

Figure 3-13 and figure 3-14 demonstrate the time evolution of deuterium depth profile, and the evolution of the pace of deuterium accumulation and the total number of deuterium trapped in the tungsten substrate, respectively. Even though, the incoming deuterium atoms may initially locate the near the surface region as seen in figure 3-10, the energy they transfer to other particles in the system can cause a chain reaction leading the further energy transfer to implanted deuterium atoms in the substrate tungsten. The implanted deuterium gained enough energy to move could leave the tungsten substrate from the surface like shown in figure 3-12 or go to the deeper region of the tungsten substrate as seen in figure 3-13. The accumulation pace of deuterium is measured by dividing the number of deuterium trapped in tungsten substrate by the total number of deuterium bombarded the tungsten over a constant time. The pace of deuterium accumulation shows a decrease in time even though the absorption rate of deuterium rises as shown in figure 3-9. In other words, while the total absorbed deuterium in tungsten substrate increases in time, the number of deuterium escaping from the surface of tungsten, as depicted in figure 3-12, also rises. This increase in the escaping deuterium causes the decrease in the pace of deuterium accumulation in tungsten substrate.

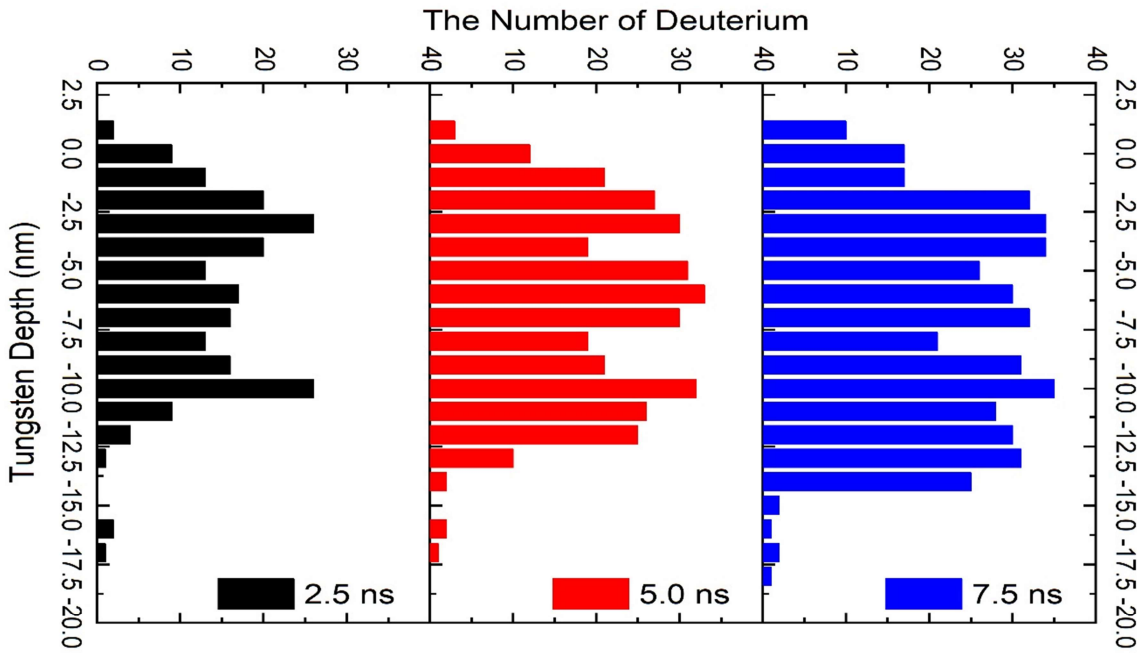

Figure 3-13 The depth profile of deuterium in tungsten substrate at 1000 K bombarded by 100 eV deuterium after various bombardment time

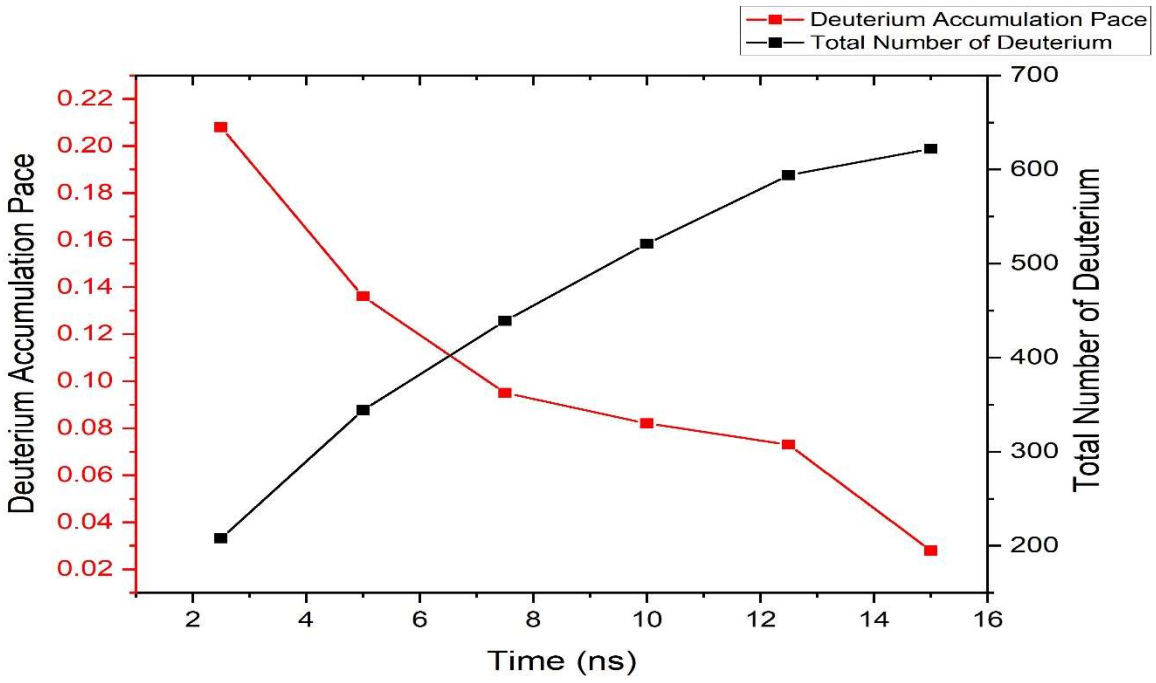

Figure 3-14 Time evolution of deuterium accumulation pace and the total number of deuterium trapped in tungsten substrate bombarbed by 100 eV deuterium

4. CONCLUSION

The deuterium trapping in tungsten substrate was studied by using molecular dynamics method. LAMMPS code developed by Sandia National Laboratory employed to determine how the parameters such as the angle or the energy of the incident particle, the temperature of the tungsten substrate, and the concentration of implanted deuterium influenced the deuterium trapping in tungsten. Various non-cumulative and cumulative simulations were run to analyze the deuterium trapping in tungsten.

The angle dependence of the absorption rate of deuterium in tungsten was studied by non-cumulative bombardment. In this bombardment, a tungsten substrate at 600 K were bombarded by 80 eV deuterium with various angles from surface normal to 80 degree. Additionally, two tungsten substrates with different surface structure also analyzed. The absorption rate of deuterium showed that the preferential angle of deuterium trapping in tungsten, at which the absorption rate was high, is depended on the surface structure of the tungsten substrate.

The effect of the substrate temperature and the energy of incident particle were examined by non-cumulative simulations. The tungsten substrate at various temperature from 300 K to 1000 K were bombarded by deuterium with energies from 10 eV to 100 eV. The energy of the incoming particle mainly influenced the absorption rate of deuterium, the average implantation depth of the deuterium, and the average required time for incident particle to be rest. The rise in the energy of the incoming deuterium increased the absorption rate of deuterium, the average required time to rest, and the average initial implantation depth of incident particle. On the other hand, the temperature of the tungsten substrate might influence the absorption rate of deuterium due to higher sticking coefficient for the deuterium at low energy. Additionally, the increase in the substrate temperature slightly decreased the energy lost per collision between deuterium and tungsten atoms.

Finally, the effect of implanted deuterium was studied by using combination of non-cumulative (for analyzing) and cumulative (for pre-irradiation) bombardments. The tungsten substrate at 1000 K was bombarded by 100 eV deuterium. The tungsten substrates with various deuterium

concentrations from 2.5 to 5.2 percent were analyzed. While the rise in the deuterium concentration increased the absorption rate of deuterium, it reduced the average initial implantation depth of deuterium and the required time to rest for incident particle because of the interaction between incident deuterium and implanted deuterium. And the probability of this interaction highly depended on the energy of incident deuterium and deuterium concentration in tungsten substrate. As a result of interaction between deuterium atoms, the implanted deuterium could gain enough energy to become mobile again and they could penetrate deeper side of tungsten substrate or could leave the tungsten substrate from the surface which decreased the number of deuterium trapped in the tungsten.

In the future studies, the deuterium tungsten simulation may be extended by adding helium to have more realistic case relevant to fusion reactor conditions. Existence of helium may significantly influence the interaction between deuterium and tungsten. Additionally, by combining Monte Carlo method with molecular dynamics, a hybrid simulation, the more realistic result of interaction between helium, deuterium, and tungsten can be studied for longer time periods.

APPENDIX 1.

WH.Tersoff Potential:

```
W  W  W  1.0 0.00188227 0.45876 2.14969 0.17126 0.277800 1.0 1.0 1.4112458892
306.4996797422 3.50 0.30 2.7195837282 3401.4744241377

W  W  H  1.0 0.00540000 0.00000 1.78800 0.82550 -0.38912 0.0 0.0
0.0000000000  0.0000000000 2.15 0.20 0.0000000000 0.0000000000

W  H  H  1.0 0.00540000 0.00000 1.78800 0.82550 -0.38912 1.0 1.0 1.9276620837
384.8728524449 2.15 0.20 2.4074571763 705.7464150077

W  H  W  1.0 0.00188227 0.45876 2.14969 0.17126 0.277800 0.0 0.0 0.0000000000
0.0000000000 3.50 0.30 0.0000000000 0.0000000000

H  H  H  1.0 12.3300000 4.00000 0.00000 1.00000 -1.00000 1.0 1.0 1.7956314729
31.3793415132 1.40 0.30 4.2075236673 80.0703477291

H  H  W  1.0 0.00540000 0.00000 1.78800 0.82550 -0.38912 0.0 0.0 0.0000000000
0.0000000000 2.15 0.20 0.0000000000 0.0000000000

H  W  W  1.0 0.00540000 0.00000 1.78800 0.82550 -0.38912 1.0 1.0 1.9276620837
384.8728524449 2.15 0.20 2.4074571763 705.7464150077

H  W  H  1.0 12.3300000 0.00000 0.00000 1.00000 -1.00000 0.0 0.0 0.0000000000
0.0000000000 1.40 0.30 0.0000000000 0.0000000000
```

APPENDIX 2.

Substrate Creation Script:

```
clear

variable temperature equal 1000
variable thisfile string W${temperature}K.txt
variable restartfile string Base_W${temperature}K
variable dumptrjfile string W${temperature}K.*.lammpstrj.gz
variable dumpimagefile string W${temperature}K.*.jpg


# --- Initional variables --- #
units metal
dimension 3
boundary p p f
atom_style atomic
atom_modify map array

# --- Geometry in unit A --- #
variable max_x equal 25.342
variable max_y equal 25.342
variable min_z equal -200
variable mid_z equal -60
variable max_z equal 80
variable fixed_W_topline equal -190
variable D_init_position equal 30
variable berendsen_xmin equal 3.165
variable berendsen_xmax equal ${max_x}-3.165
variable berendsen_ymin equal 3.165
variable berendsen_ymax equal ${max_y}-3.165
variable berendsen_zmin equal ${fixed_W_topline}+12.66
variable berendsen_zmax equal 3.165

# --- Steps --- #
variable Wtemp_rescall_step equal 6000

# --- Create W atoms --- #
lattice bcc 3.165
region rgn_everything block 0 ${max_x} 0 ${max_y} ${min_z} ${max_z} units box
create_box 3 rgn_everything
region rgn_w_upper_lattice block 0.3165 ${max_x} 0.3165 ${max_y}
${mid_z}+1.5825 0.0 units box
lattice bcc 3.165 orient x 1 0 0 orient y 0 1 0 orient z 0 0 1
create_atoms 1 region rgn_w_upper_lattice
```

```
region rgn_w_lower_lattice block 0.3165 ${max_x} 0.3165 ${max_y} ${min_z}
${mid_z}-1.5825 units box
lattice bcc 3.165 orient x 1 0 0 orient y 0 1 0 orient z 0 0 1
create_atoms 2 region rgn_w_lower_lattice

# --- Mass --- #
variable mass_W equal 183.84
variable mass_D equal 2.01410178
mass 1 ${mass_W}
mass 2 ${mass_W}
mass 3 ${mass_D}

# --- W temp --- #
variable W_temp equal ${temperature} #kelvin

# --- Potential --- #
pair_style tersoff
pair_coeff * * HW.tersoff W W H
neighbor 2.0 bin
neigh_modify delay 0 every 1 check yes

# --- Fix the bottom W --- #
region rgn_fixed_W block 0 ${max_x} 0 ${max_y} ${min_z} ${fixed_W_topline}
units box
group grp_fixed_W region rgn_fixed_W
fix zeroforce grp_fixed_W setforce 0 0 0

# --- berendsen group, must define before the rescalling --- #
region rgn_1 block ${berendsen_xmin} ${berendsen_xmax} &
 ${berendsen_ymin} ${berendsen_ymax} &
 ${berendsen_zmin}  ${berendsen_zmax} units box
group grp_1 region rgn_1
group grp_berendsen_W subtract all grp_1 grp_fixed_W
group grp_1 delete

# ---- Init W temp ---- #
group grp_mobile_W subtract all grp_fixed_W
velocity grp_mobile_W create ${W_temp} 12345 rot yes dist gaussian

# ---- Temp rescalling ----
fix 1 all nve
fix 2 grp_mobile_W temp/rescale 100 ${W_temp} ${W_temp} 0.1 1.0

compute cmp_Wtemp grp_mobile_W temp

timestep 0.01

thermo_style custom step temp pe c_cmp_Wtemp cpu tpcpu spcpu
thermo_modify lost warn
thermo 25
```

```
dump 1 all atom 100 W${temperature}K.*.LAMMPStrj.gz
dump 2 all image ${Wtemp_rescall_step} W${temperature}K.*.jpg type type size
1024 1280 &
zoom 2.0 box yes 0.005 axes yes 0.5 0.05 view 60 -30
dump_modify 2 adiam 1 2.0 adiam 2 2.0


run ${Wtemp_rescall_step}

unfix 1
unfix 2
unfix zeroforce

write_restart ${restartfile}
```

APPENDIX 3.

Non-cumulative Bombardment Script:

```
clear

variable temperature equal 800
variable Denergy equal 10
variable thisfile string W${temperature}K_${Denergy}eV.txt
variable restartfile string Base_W${temperature}K
variable logfile string result_W${temperature}K_D${Denergy}eV.log
variable dumptrjfile string W${temperature}K.*.lammpstrj.gz
variable dumpimagefile string W${temperature}K.*.jpg

# --- Geometry in unit A --- #
variable max_x equal 25.342
variable max_y equal 25.342
variable min_z equal -200
variable mid_z equal -90
variable max_z equal 80
variable fixed_W_topline equal -190
variable D_init_position equal 15

# --- Steps --- #
variable total_cycles equal 1000
variable cycle_steps equal 10000
variable check_interval equal 50

region rgn_everything block 0 ${max_x} 0 ${max_y} ${min_z} ${max_z} units box
create_box 3 rgn_everything

# --- Mass --- #
variable mass_W equal 183.84
variable mass_D equal 2.01410178

mass 1 ${mass_W}
mass 2 ${mass_W}
mass 3 ${mass_D}

# --- D energy and W temp --- #
variable W_temp equal ${temperature} #kelvin
variable D_energy equal ${Denergy} #eV
variable D_speed equal (-1)*sqrt(${D_energy}*1.602e-19*2.0/(${mass_D}*1.661e-
27))*1.e10/1.e12 # A/ps

#  Bombardment begins

# --- D velocity --- #
```

```
variable D_azi_angle equal random(0,6.2831852,24642)
variable D_polar_angle equal 0 # perpendecular to surface

variable rn equal 0.0

variable D_x equal random(0,${max_x},13531)
variable D_y equal random(0,${max_y},13531)
variable D_z equal ${D_init_position}

variable D_vx equal ${D_speed}*sin(${D_polar_angle})*cos(${D_azi_angle})
variable D_vy equal ${D_speed}*sin(${D_polar_angle})*sin(${D_azi_angle})
variable D_vz equal ${D_speed}*cos(${D_polar_angle})

variable Dz_bottom equal ${D_init_position}-0.5
variable Dz_top equal ${D_init_position}+0.5

region rgn_D_born block 0 ${max_x} 0 ${max_y} ${Dz_bottom} ${Dz_top} units
box


# --- Shooting the Deuterium --- #

variable i loop ${total_cycles} #cycle_loop
variable n loop ${total_cycles} #count of trapped D
variable r loop ${total_cycles} #reflection from surface

variable Refcheck equal 0

label cycle_loop

#--- re-set up the calculation

clear

read_restart ${restartfile}

pair_style tersoff
pair_coeff * * HW.tersoff W W H
neighbor 2.0 bin
neigh_modify delay 0 every 1 check yes

timestep 0.0005
reset_timestep 0

fix 1 all nve
fix 2 grp_berendsen_W temp/berendsen ${W_temp} ${W_temp} 0.01
fix zeroforce grp_fixed_W setforce 0 0 0
region rgn_check_flying_atoms block 0 ${max_x} 0 ${max_y} ${Dz_bottom}
${max_z} units box
```

```
# --- set-up completed --- #

print "============================>>> Shooting $i -th D..."

create_atoms 3 single ${D_x} ${D_y} ${D_z} units box

group grp_all_D type 3
compute Dtemp grp_all_D ke
compute_modify Dtemp dynamic yes # D temp
compute cmp_Wtemp grp_mobile_W temp # W temp

variable alldke equal c_Dtemp # kinetic energy of D
variable dzz equal xcm(grp_all_D,z) #z coord of D

thermo_style custom step temp pe c_cmp_Wtemp c_Dtemp v_dzz cpu tpcpu spcpu
thermo_modify lost warn
thermo 50

# get random number --------
    variable rn equal ${D_azi_angle}
    variable rnp equal ${D_polar_angle}
    variable D_vx equal ${D_speed}*sin(${rnp})*cos(${rn})
    variable D_vy equal ${D_speed}*sin(${rnp})*sin(${rn})
    variable D_vz equal ${D_speed}*cos(${rnp})

velocity grp_all_D set ${D_vx} ${D_vy} ${D_vz} units box

group grp_all_D type 3
group grp_all_W type 1 2

variable dx equal xcm(grp_all_D,x)
variable dy equal xcm(grp_all_D,y)
variable dz equal xcm(grp_all_D,z)
print "The $i -th D initial location is ${dx} ${dy} ${dz}"

label cont_run
variable steps equal step
if "${steps} > ${cycle_steps}" then "jump ${thisfile} writeD"

run ${check_interval}

# check D lost
variable numD equal count(grp_all_D)
if "${numD} <= 0" then "jump ${thisfile} writeD" # D lost

# else: check D reflection
variable Dzz equal xcm(grp_all_D,z)
if "${Dzz} > ${Dz_top}" then "variable Refcheck equal 1" &
"delete_atoms group grp_all_D" &
"jump ${thisfile} writeD" # D reflected
```

```
# else: check D energy
if "${alldke} >= 0.5" then "jump ${thisfile} cont_run" # Contunue to run

# else: record

label writeD
delete_atoms region rgn_check_flying_atoms

variable Didx equal $n
variable Ref equal $r

if "${numD} <= 0" then "variable Didx equal 0"
if "${Refcheck} == 0" then "variable Ref equal 0"

variable Dzz equal xcm(grp_all_D,z)
variable Wnum equal count(grp_all_W)
variable Dnum equal count(grp_all_D)

print "-----------> Recording $n -th D... "
print "${Didx} ${i} ${Dzz} ${alldke} ${steps} ${Dnum} ${Wnum} ${Ref}" append
${logfile}

if "${numD} > 0" then " next n"
if "${Refcheck} == 1" then "next r" &
"variable Refcheck equal 0"

next i
jump ${thisfile} cycle_loop
```

APPENDIX 4.

Cumulative Bombardment Script:

```
clear

variable temperature equal 1000
variable Denergy equal 100
variable thisfile string W${temperature}K_${Denergy}eV.txt
variable restartfile string Base_W${temperature}K
variable logfile string result_W${temperature}K_D${Denergy}eV.log
variable dumptrjfile string W${temperature}K.*.lammpstrj.gz
variable dumpimagefile string W${temperature}K.*.jpg

# --- Geometry in unit A --- #
variable max_x equal 25.342
variable max_y equal 25.342
variable min_z equal -200
variable mid_z equal -90
variable max_z equal 80
variable fixed_W_topline equal -190
variable D_init_position equal 40

# --- Steps --- #
variable Wtemp_rescall_step equal 2000
variable total_cycles equal 3000
variable cycle_steps equal  5000
variable restart equal 10

# ---Create Simulation box--- #
#region rgn_everything block 0 ${max_x} 0 ${max_y} ${min_z} ${max_z} units
box
#create_box 3 rgn_everything
read_restart ${restartfile}

# ---Mass--- #
variable mass_W equal 183.84
variable mass_D equal 2.01410178
mass 1 ${mass_W}
mass 2 ${mass_W}
mass 3 ${mass_D}

# ---D energy and W temp--- #
variable W_temp equal ${temperature} #kelvin
variable D_energy equal ${Denergy} #eV
variable D_speed equal (-1)*sqrt(${D_energy}*1.602e-19*2.0/(${mass_D}*1.661e-
27))*1.e10/1.e12 # A/ps
```

```
# ---Potential--- #
pair_style tersoff
pair_coeff * * HW.tersoff W W H
neighbor 2.0 bin
neigh_modify delay 0 every 1 check yes

# ---Fix the bottom W--- #

#group grp_fixed_W region rgn_fixed_W
fix zeroforce grp_fixed_W setforce 0 0 0

# ---- Init W temp ----
group grp_mobile_W subtract all grp_fixed_W
velocity grp_mobile_W create ${W_temp} 12345 rot yes dist gaussian

# ---- Temp rescalling ----
fix 1 all nve
fix 2 grp_berendsen_W temp/berendsen ${W_temp} ${W_temp} 0.01

#==== ==== ====
#  Bombardment begins
#==== ==== ====

#---- D velocity ----
variable D_azi_angle equal random(0,6.2831852,13531)
variable D_polar_angle equal 0

variable rn equal 0.0

variable D_x equal random(0,${max_x},13531)
variable D_y equal random(0,${max_y},13531)
variable D_z equal ${D_init_position}

variable Dz_bottom equal ${D_init_position}-0.5
variable Dz_top equal ${D_init_position}+0.5

region rgn_D_born block 0 ${max_x} 0 ${max_y} ${Dz_bottom} ${Dz_top} units
box

reset_timestep 0
timestep 0.0005

#---- SHOOTING THE D ------
group grp_all_D type 3
group grp_rgn_born region rgn_D_born
group grp_D_born intersect grp_rgn_born grp_all_D

variable Dke equal ke(grp_D_born) #kinetic energy
variable dzz equal xcm(grp_all_D,z) #z coord of D
compute cmp_Wtemp grp_mobile_W temp
```

```
thermo_style custom step temp c_cmp_Wtemp v_Dke v_dzz cpu tpcpu spcpu
thermo_modify lost warn
thermo 1000

dump D-text all atom ${cycle_steps} ${dumptrjfile}
dump D-images all image ${cycle_steps} ${dumpimagefile} type type size 1024
1280 &
zoom 2.0 box yes 0.005 axes yes 0.5 0.05 view 60 -30
dump_modify D-images adiam 1 2.0 adiam 2 2.0

variable i loop ${total_cycles} #cycle_loop

label cycle_loop
print "====>>>> Shooting $i -th D..."
create_atoms 3 single ${D_x} ${D_y} ${D_z} units box
group grp_all_D type 3

# get random number --------
    variable rn equal ${D_azi_angle}
    variable rnp equal ${D_polar_angle}
    variable D_vx equal ${D_speed}*sin(${rnp})*cos(${rn})
    variable D_vy equal ${D_speed}*sin(${rnp})*sin(${rn})
    variable D_vz equal ${D_speed}*cos(${rnp})

group grp_rgn_born delete
group grp_D_born delete

group grp_rgn_born region rgn_D_born
group grp_D_born intersect grp_rgn_born grp_all_D

velocity grp_D_born set ${D_vx} ${D_vy} ${D_vz} units box

variable dx equal xcm(grp_all_D,x)
variable dy equal xcm(grp_all_D,y)
variable dz equal xcm(grp_all_D,z)

print "The $i -th D initial location is ${dx} ${dy} ${dz}"

run ${cycle_steps}

if "${i} == ${restart}" then &
"write_restart $i${restartfile}" &
"variable restart equal ${restart}+10"

next i
jump ${thisfile} cycle_loop
```

REFERENCES

[1] "https://www.iaea.org." .

[2] J. Küppers, "The hydrogen surface chemistry of carbon as a plasma facing material," *Surf. Sci. Rep.*, vol. 22, no. 7–8, pp. 249–321, Jan. 1995.

[3] F. L. Tabarés, "Tritium inventory control during ITER operation under carbon plasma-facing components by nitrogen-based plasma chemistry: A review," *Plasma Sources Sci. Technol.*, vol. 22, no. 3, pp. 1–12, 2013.

[4] D. Hildebrandt, M. Akbi, B. Jüttner, and W. Schneider, "Deuterium trapping in divertor tiles of ASDEX-Upgrade," *J. Nucl. Mater.*, vol. 266, pp. 532–537, Mar. 1999.

[5] J. Linke, "High Heat Flux Performance of Plasma Facing Materials and Components Under," *Fusion Sci. Technol.*, vol. 53, no. November, pp. 278–287, 2008.

[6] J. Roth *et al.*, "Recent analysis of key plasma wall interactions issues for ITER," *J. Nucl. Mater.*, vol. 390–391, no. 1, pp. 1–9, 2009.

[7] D. Whitley, J., Wilson, K., and Buchenauer, "Metallic Materials as Plasma Facing Components - A Review.," *J. Nucl. Mater.*, vol. 155–157, pp. 82–94, 1988.

[8] M. Poon, R. G. Macaulay-Newcombe, J. W. Davis, and A. A. Haasz, "Flux dependence of deuterium retention in single crystal tungsten," *J. Nucl. Mater.*, vol. 307–311, pp. 723–728, 2002.

[9] X. Yang and A. Hassanein, "Molecular dynamics simulation of deuterium trapping and bubble formation in tungsten," *J. Nucl. Mater.*, vol. 434, no. 1–3, pp. 1–6, 2013.

[10] K. Tokunaga *et al.*, "Blister formation and deuterium retention on tungsten exposed to low energy and high flux deuterium plasma," *J. Nucl. Mater.*, vol. 337–339, no. 1–3, pp. 887–891, 2005.

[11] W. M. Shu, A. Kawasuso, and T. Yamanishi, "Recent findings on blistering and deuterium retention in tungsten exposed to high-fluence deuterium plasma," *J. Nucl. Mater.*, vol. 386–388, pp. 356–359, 2009.

[12] "http://ambermd.org/." .

[13] "https://lammps.sandia.gov/." .

[14] "http://www.ks.uiuc.edu/Research/namd/." .

[15] K. C. Mundim, L. A. C. Malbouisson, S. Dorfman, D. Fuks, J. Van Humbeeck, and V. Liubich, “Diffusion properties of tungsten from atomistic simulations with ab initio potentials,” *J. Mol. Struct. THEOCHEM*, vol. 539, no. 1–3, pp. 191–197, 2001.

[16] A. K. Rappé, C. J. Casewit, K. S. Colwell, W. A. Goddard, and W. M. Skiff, “UFF, a Full Periodic Table Force Field for Molecular Mechanics and Molecular Dynamics Simulations,” *J. Am. Chem. Soc.*, vol. 114, no. 25, pp. 10024–10035, 1992.

[17] I. S. Landman, “Simulation of multi-atomic interactions in H-O-W system with the MD code CADAC,” *Fusion Eng. Des.*, vol. 75–79, pp. 417–421, 2005.

[18] I. S. Landman and H. Wuerz, “Molecular dynamics simulations of the effect of deuterium on tungsten erosion by oxygen,” in *Journal of Nuclear Materials*, 2003, vol. 313, pp. 77–81.

[19] Z. Fan, W. Chen, V. Vierimaa, and A. Harju, “Efficient molecular dynamics simulations with many-body potentials on graphics processing units,” *Comput. Phys. Commun.*, vol. 218, pp. 10–16, 2017.

[20] M. W. Finnis and J. E. Sinclair, “A simple empirical N-body potential for transition metals,” *Philos. Mag. A*, vol. 50, no. 1, pp. 45–55, 1984.

[21] G. J. Ackland and R. Thetford, “An improved N-body semi-empirical model for body-centred cubic transition metals,” *Philos. Mag. A*, vol. 56, no. 1, pp. 15–30, 1987.

[22] R. A. Johnson and D. J. Oh, “Analytic embedded atom method model for bcc metals,” *J. Mater. Res.*, vol. 4, no. 5, pp. 1195–1201, 1989.

[23] S. M. Foiles, “Interatomic interactions for Mo and W based on the low-order moments of the density of states,” *Phys. Rev. B*, vol. 48, no. 7, pp. 4287–4298, 1993.

[24] L. T. Kong, X. Y. Li, W. S. Lai, J. B. Liu, and B. X. Liu, “Interfacial reaction of W/Cu examined by an n-body potential through molecular dynamics simulations,” *Jpn. J. Appl. Phys.*, vol. 41, no. 7R, pp. 4503–4508, 2002.

[25] J. Wang, Y. L. Zhou, M. Li, and Q. Hou, “A modified W-W interatomic potential based on ab initio calculations,” *Model. Simul. Mater. Sci. Eng.*, vol. 22, no. 1, p. 15, 2014.

[26] M. C. Marinica *et al.*, “Interatomic potentials for modelling radiation defects and dislocations in tungsten,” *J. Phys. Condens. Matter*, vol. 25, no. 39, p. 15, 2013.

[27] N. Juslin and B. D. Wirth, “Interatomic potentials for simulation of He bubble formation in W,” *J. Nucl. Mater.*, vol. 432, no. 1–3, pp. 61–66, 2013.

[28] Y. R. Wang and D. B. Boercker, “Effective interatomic potential for body-centered-cubic metals,” *J. Appl. Phys.*, vol. 78, no. 1, pp. 122–126, 1995.

[29] W. Hu, X. Shu, and B. Zhang, “Point-defect properties in body-centered cubic transition metals with analytic EAM interatomic potentials,” *Comput. Mater. Sci.*, vol. 23, no. 1–4, pp. 175–189, 2002.

[30] N. Juslin *et al.*, “Analytical interatomic potential for modeling nonequilibrium processes in the W-C-H system,” *Journal of Applied Physics*, vol. 98, no. 12. pp. 123520–123532, 2005.

[31] M. Mrovec, R. Gröger, A. G. Bailey, D. Nguyen-Manh, C. Elsässer, and V. Vitek, “Bond-order potential for simulations of extended defects in tungsten,” *Phys. Rev. B*, vol. 75, no. 10, pp. 1–17, 2007.

[32] K. O. E. Hnriksson, K. Nordland, J. Keinonen, D. Sundholm, and M. Patzschke, “Simulations of the Initial Stages of Blistering in Helium Implanted Tungsten,” *Phys. Scr.*, vol. T108, pp. 95–98, 2004.

[33] Q. Xie and P. Chen, “Semiempirical tight-binding interatomic potentials based on the Hubbard model,” *Phys. Rev. B - Condens. Matter Mater. Phys.*, vol. 56, no. 9, pp. 5235–5242, 1997.

[34] X. C. Li, X. Shu, Y. N. Liu, F. Gao, and G. H. Lu, “Modified analytical interatomic potential for a W-H system with defects,” *J. Nucl. Mater.*, vol. 408, no. 1, pp. 12–17, 2011.

[35] X. Duan, B. Zhou, Y. Wen, R. Chen, H. Zhou, and B. Shan, “Lattice inversion modified embedded atom method for bcc transition metals,” *Comput. Mater. Sci.*, vol. 98, no. C, pp. 417–423, 2015.

[36] M. I. Baskes, “Modified embedded-atom potentials for cubic materials and impurities,” *Phys. Rev. B*, vol. 46, no. 5, pp. 2727–2742, 1992.

[37] W. Xu and J. B. Adams, “Fourth moment approximation to tight binding: application to bcc transition metals,” *Surf. Sci.*, vol. 301, no. 1–3, pp. 371–385, 1994.

[38] A. Carlsson, “Angular forces in group-VI transition metals: Application to W(100),” *Phys. Rev. B*, vol. 44, no. 13, pp. 6590–6597, 1991.

[39] H. Fan *et al.*, “Surface degeneration of W crystal irradiated with low-energy hydrogen ions,” *Sci. Rep.*, vol. 6, no. December 2015, p. 23738, 2016.

[40] Y. Z. Jia, W. Liu, B. Xu, S. L. Qu, L. Q. Shi, and T. W. Morgan, “Subsurface deuterium bubble formation in W due to low-energy high flux deuterium plasma exposure,” *Nucl. Fusion*, vol. 57, no. 3, p. 034003, 2017.

[41] Y. Z. Jia *et al.*, “Nanostructures and pinholes on W surfaces exposed to high flux D plasma at high temperatures,” *J. Nucl. Mater.*, vol. 463, pp. 312–315, 2015.

[42] H. Y. Xu *et al.*, “Blistering on tungsten surface exposed to high flux deuterium plasma,” *J. Nucl. Mater.*, vol. 471, pp. 51–58, 2016.

[43] G. N. Luo, K. Umstadter, W. M. Shu, W. Wampler, and G. H. Lu, “Behavior of tungsten with exposure to deuterium plasmas,” *Nucl. Instruments Methods Phys. Res. Sect. B Beam Interact. with Mater. Atoms*, vol. 267, no. 18, pp. 3041–3045, 2009.

[44] H. J. C. Berendsen, J. P. M. Postma, W. F. Van Gunsteren, A. Dinola, and J. R. Haak, “Molecular dynamics with coupling to an external bath,” *J. Chem. Phys.*, vol. 81, no. 8, pp. 3684–3690, 1984.

[45] S. SAITO, A. M. ITO, and H. NAKAMURA, “Molecular Dynamics Simulation of the Incident Angle Dependence of Reactions between Graphene and Hydrogen Atom,” *Plasma Fusion Res.*, vol. 5, no. June 2014, pp. S2076–S2076, 2010.

[46] V. K. Alimov and J. Roth, “Hydrogen isotope retention in plasma-facing materials: Review of recent experimental results,” *Phys. Scr.*, vol. T128, pp. 6–13, 2007.

[47] X. W. Zhou, D. K. Ward, M. Foster, and J. A. Zimmerman, “An analytical bond-order potential for the copper–hydrogen binary system,” *J. Mater. Sci.*, vol. 50, no. 7, pp. 2859–2875, 2015.